Semileptonic B_{(s)} decays to excited charmed mesons with e, μ, τ and searching for new physics with R(D**)

Florian U. Bernlochner and Zoltan Ligeti

Phys. Rev. D **95**, 014022 — Published 23 January 2017

DOI: 10.1103/PhysRevD.95.014022

Semileptonic $B_{(s)}$ decays to excited charmed mesons with e, μ, τ and searching for new physics with $R(D^{**})$

Florian U. Bernlochner[1] and Zoltan Ligeti[2]

[1] *Physikalisches Institut der Rheinische Friedrich-Wilhelms-Universität Bonn, 53115 Bonn, Germany*
[2] *Ernest Orlando Lawrence Berkeley National Laboratory, University of California, Berkeley, CA 94720*

Semileptonic B meson decays into the four lightest excited charmed meson states (D_0^*, D_1^*, D_1, and D_2^*) and their counterparts with s quarks are investigated, including the full lepton mass dependence. We derive the standard model predictions for the differential branching fractions, as well as predictions for the ratios of the semi-tauonic and light lepton semileptonic branching fractions. These can be systematically improved using future measurements of the total or differential semileptonic rates to e and μ, as well as the two-body hadronic branching fractions with a pion, related by factorization to the semileptonic rate at maximal recoil. To illustrate the different sensitivities to new physics, we explore the dependence of the ratio of semi-tauonic and light-lepton branching fractions on the type-II and type-III two-Higgs-doublet model parameters, $\tan\beta$ and $m_H^\pm$, for all four states.

I. INTRODUCTION

The study of semileptonic $b \to c$ decays has been a central focus of the B factory experiments *BABAR* and Belle, as well as LHCb. Such decays are important for the measurement of the Cabibbo-Kobayashi-Maskawa (CKM) matrix element $|V_{cb}|$ and are also probes of physics beyond the standard model (SM). Theoretically, exclusive semileptonic B decays to D and D^* are well understood and inclusive semileptonic $B \to X_c \ell \bar{\nu}$ decay has also been the focus of extensive research. Semileptonic B decays to excited charmed mesons received less attention, but are important for the following reasons.

1. Recently, *BABAR*, Belle, and LHCb reported discrepancies from the SM predictions in semi-tauonic decays compared to the $l = e$, μ light lepton final states [1–4]. Their average shows a disagreement with the SM expectation at the 4σ level [5]. This tension is intriguing, because it occurs in a tree-level SM process, and most new physics explanations require new states at or below 1 TeV [6].

   Semileptonic decays into excited charmed mesons with light leptons are an important background, and their better understanding is needed to improve the precision of these ratios.

2. Determinations of the CKM matrix element $|V_{cb}|$ from exclusive and inclusive semileptonic B decays exhibit a nearly 3σ tension [5]. Decays involving heavier charmed mesons are an important background of untagged exclusive measurements, and are also important in inclusive $|V_{cb}|$ measurements since efficiency and acceptance effects are modeled using a mix of exclusive decay modes that includes decays into excited charmed mesons.

3. Semi-tauonic decays into excited charmed mesons provide a complementary probe of the enhancements observed in the semi-tauonic decays to D and D^*. Moreover, the measured semi-tauonic decays to D and D^* appear to saturate the inclusive $\bar{B} \to X\,\tau\bar{\nu}$ rate [6]. This motivates measuring this decay, and if the enhancement is verified, new physics modifying the $D^{(*)}$ rates must also fit the semi-tauonic rates for higher mass charm states.

Heavy quark symmetry [7] provides some model independent predictions for exclusive semileptonic B decays to excited charmed mesons, even including $\Lambda_{\rm QCD}/m_{c,b}$ corrections [8]. Approximations based on those results constitute the LLSW model [9], used in many experimental analyses. The key observation was that some of the $\Lambda_{\rm QCD}/m_{c,b}$ corrections to semileptonic form factors at zero recoil are determined by the masses of orbitally excited charmed mesons [8, 9].

The isospin averaged masses and widths of the four lightest excited D meson states are shown in Table I. In the quark model, they correspond to combining the heavy quark and light quark spins with $L = 1$ orbital angular momentum. In the heavy quark limit, the spin-parity of the light degrees of freedom, $s_l^{\pi_l}$, is a conserved quantum number [12]. This spectroscopy is important, because in addition to the impact on the kinematics, they give important information on HQET matrix elements and

Particle	$s_l^{\pi_l}$	J^P	m (MeV)	Γ (MeV)
D_0^*	$\frac{1}{2}^+$	0^+	2330	270
D_1^*	$\frac{1}{2}^+$	1^+	2427	384
D_1	$\frac{3}{2}^+$	1^+	2421	34
D_2^*	$\frac{3}{2}^+$	2^+	2462	48
B_1	$\frac{3}{2}^+$	1^+	5727	28
B_2^*	$\frac{3}{2}^+$	2^+	5739	23

TABLE I. Isospin averaged masses and widths of some excited D mesons, rounded to 1 MeV. For the $\frac{3}{2}^+$ states we averaged the PDG with LHCb measurements [10, 11] not included in the PDG. The D_0^* mass is discussed in the text; see Table II.

m (MeV)	Γ (MeV)	reference
2405 ± 36	274 ± 45	FOCUS [13]
2308 ± 36	276 ± 66	Belle [14]
2297 ± 22	273 ± 49	*BABAR* [15]
2360 ± 34	255 ± 57	LHCb [16]
2330 ± 15	270 ± 26	our average

TABLE II. Isospin averaged $D_0^*(2400)$ masses and widths. The LHCb measurement [16] is missing from the PDG.

$s_l^{\pi_l}$	Particles	$\overline{m}$ (MeV)	Particles	$\overline{m}$ (MeV)
$\frac{1}{2}^-$	D, D^*	1973	B, B^*	5313
$\frac{1}{2}^+$	D_0^*, D_1^*	2403	B_0^*, B_1^*	—
$\frac{3}{2}^+$	D_1, D_2^*	2445	B_1, B_2^*	5734

TABLE III. Isospin and heavy quark spin symmetry averaged masses of lightest B and D multiplets (with weights $2J+1$).

the QCD dynamics. The level of agreement between the measurements of the masses and widths of the excited D states in the top 4 rows of Table I is not ideal. In particular, the mass of the $D_0^*(2400)$ varies in published papers by 100 MeV, as shown in Table II. The confidence level of our mass average in the last row is 5%.

The masses of a heavy quark spin symmetry doublet of hadrons, $H_\pm$, with total spin $J_\pm = s_l \pm \frac{1}{2}$ can be expressed in HQET as

$$m_{H_\pm} = m_Q + \bar{\Lambda}^H - \frac{\lambda_1^H}{2m_Q} \pm \frac{n_\mp\, \lambda_2^H}{2m_Q} + \dots\,, \qquad (1)$$

where $n_\pm = 2J_\pm + 1$ is the number of spin states of each hadron, and the ellipsis denote terms suppressed by more powers of $\Lambda_{\rm QCD}/m_Q$. The parameter $\bar{\Lambda}^H$ is the energy of the light degrees of freedom in the $m_Q \to \infty$ limit, and plays an important role, as it is related to the semileptonic form factors [8, 9]. We use the notation $\bar{\Lambda}$, $\bar{\Lambda}'$, and $\bar{\Lambda}^*$ for the $\frac{1}{2}^-$, $\frac{3}{2}^+$, and $\frac{1}{2}^+$ doublets, respectively. The λ_1^H and λ_2^H parameters are related to the heavy quark kinetic energy and chromomagnetic energy in hadron H.

The current data suggest that the $m_{D_1^*} - m_{D_0^*}$ mass splitting is substantially larger than the $m_{D_2^*} - m_{D_1}$ splitting. This possibility was not considered in Refs. [8, 9], since at that time both of these mass splittings were about 40 MeV. The smallness of $m_{D_2^*} - m_{D_1}$ and $m_{D_1^*} - m_{D_0^*}$ compared to $m_{D^*} - m_D \simeq 140\,\text{MeV}$ was taken as an indication that the chromomagnetic operator matrix elements are suppressed for the four D^{**} states, in agreement with quark model predictions. We explore the consequences of relaxing this constraint.

The isospin and heavy quark spin symmetry averaged masses in Table III and Eq. (1.10) in Ref. [9], which is valid to $\mathcal{O}(\Lambda_{\rm QCD}^3/m_{c,b}^2)$, yield $\bar{\Lambda}' - \bar{\Lambda} = 0.40\,\text{GeV}$ (using $m_b = 4.8\,\text{GeV}$ and $m_c = 1.4\,\text{GeV}$, but the sensitivity to this is small). While the masses of the broad D_0^* and D_1^* states changed substantially since the 1990s, their $2J+1$ weighted average mass is essentially unchanged compared to Ref. [9]. We estimate $\bar{\Lambda}' - \bar{\Lambda}^* \simeq 0.04\,\text{GeV}$ from Table III. We summarize the parameters used in Table IV. The uncertainty of $\bar{\Lambda}$ is substantially greater than that of $\bar{\Lambda}' - \bar{\Lambda}$ and $\bar{\Lambda}' - \bar{\Lambda}^*$, but as we see below, our results are less sensitive to $\bar{\Lambda}$ than to these differences. The parameters with s subscripts in Table IV are relevant for $B_s \to D_s^{**}\ell\bar{\nu}$ discussed in Sec. IV.

Parameter	$\bar{\Lambda}$	$\bar{\Lambda}'$	$\bar{\Lambda}^*$	$\bar{\Lambda}_s$	$\bar{\Lambda}_s'$	$\bar{\Lambda}_s^*$
Value [GeV]	0.40	0.80	0.76	0.49	0.90	0.77

TABLE IV. The HQET parameter estimates used.

Another effect suppressed in the heavy quark limit and neglected in Refs. [8, 9], is the mixing between D_1 and D_1^*. It was recently argued that this could be substantial [17]. However, even a small mixing of the D_1 with the much broader D_1^* would yield $\Gamma_{D_1} > \Gamma_{D_2^*}$, in contradiction with the data, which suggests that this $\Lambda_{\rm QCD}/m_c$ effect may be small [18–20]. Until the masses are unambiguously measured, we neglect the effects of this mixing, which we expect to be modest, and leave it for another study, should future data suggest that it is important.

The rest of this paper is organized as follows. Section II reviews the $B \to D^{**}\,\ell\,\bar{\nu}$ decays to the four states collectively denoted

$$D^{**} = \{D_0^*,\, D_1^*,\, D_1,\, D_2^*\}\,, \qquad (2)$$

and provides expressions for these decay rates with the full lepton mass dependence. In Sec. II B the expansion of the form factors based on heavy quark symmetry [8, 9] is briefly reviewed. Section III summarizes the experimental analysis to determine the leading Isgur-Wise function normalization and slope, and we obtain predictions for the ratios of semileptonic rates for τ and light leptons,

$$R(D^{**}) = \frac{\mathcal{B}(B \to D^{**}\tau\,\bar{\nu})}{\mathcal{B}(B \to D^{**} l\,\bar{\nu})}\,, \qquad l = e, \mu\,. \qquad (3)$$

Section IV studies predictions for $B_s \to D_s^{**}\ell\bar{\nu}$. Section V explores extensions of the SM with scalar currents. Predictions for the rates and $R(D^{**})$ are derived to illustrate the complementary sensitivity of each mode. Section VI summarizes our main findings.

II. THE $B \to D^{**}\ell\,\bar{\nu}$ DECAYS IN THE SM

The effective SM Lagrangian describing $b \to c\,\ell\,\bar{\nu}$ is

$$\mathcal{L}_{\rm eff} = -\frac{4G_F}{\sqrt{2}}\, V_{cb}\, \big(\bar{c}\,\gamma_\mu P_L b\big)\big(\bar{\nu}\,\gamma^\mu P_L \ell\big) + \text{h.c.}\,, \qquad (4)$$

with the projection operator $P_L = (1-\gamma_5)/2$, G_F is the Fermi constant, and ℓ denotes any one of e, μ, τ. The matrix elements of the $B \to D^{**}$ vector and axial-vector

currents ($V^\mu = \bar{c}\,\gamma^\mu\, b$ and $A^\mu = \bar{c}\,\gamma^\mu\gamma_5\, b$) can be parameterized for the $\frac{3}{2}^+$ states as

$$\begin{aligned}
\frac{\langle D_1(v',\epsilon)|V^\mu|B(v)\rangle}{\sqrt{m_{D_1}\, m_B}} &= f_{V_1}\epsilon^{*\mu} + (f_{V_2}v^\mu + f_{V_3}v'^\mu)(\epsilon^*\cdot v)\,,\\
\frac{\langle D_1(v',\epsilon)|A^\mu|B(v)\rangle}{\sqrt{m_{D_1}\, m_B}} &= i\, f_A\, \varepsilon^{\mu\alpha\beta\gamma}\epsilon^*_\alpha v_\beta v'_\gamma\,,\\
\frac{\langle D_2^*(v',\epsilon)|A^\mu|B(v)\rangle}{\sqrt{m_{D_2^*}\, m_B}} &= k_{A_1}\,\epsilon^{*\mu\alpha}v_\alpha \\
&\quad + (k_{A_2}v^\mu + k_{A_3}v'^\mu)\,\epsilon^*_{\alpha\beta}\,v^\alpha v^\beta\,,\\
\frac{\langle D_2^*(v',\epsilon)|V^\mu|B(v)\rangle}{\sqrt{m_{D_2^*}\, m_B}} &= i\,k_V\,\varepsilon^{\mu\alpha\beta\gamma}\epsilon^*_{\alpha\sigma}v^\sigma v_\beta v'_\gamma\,,
\end{aligned} \tag{5}$$

while for the $\frac{1}{2}^+$ states

$$\begin{aligned}
\langle D_0^*(v')|V^\mu|B(v)\rangle &= 0,\\
\frac{\langle D_0^*(v')|A^\mu|B(v)\rangle}{\sqrt{m_{D_0^*}\, m_B}} &= g_+\,(v^\mu + v'^\mu) + g_-\,(v^\mu - v'^\mu)\,,\\
\frac{\langle D_1^*(v',\epsilon)|V^\mu|B(v)\rangle}{\sqrt{m_{D_1^*}\, m_B}} &= g_{V_1}\epsilon^{*\mu} + (g_{V_2}v^\mu + g_{V_3}v'^\mu)\,(\epsilon^*\cdot v)\,,\\
\frac{\langle D_1^*(v',\epsilon)|A^\mu|B(v)\rangle}{\sqrt{m_{D_1^*}\, m_B}} &= i\,g_A\,\varepsilon^{\mu\alpha\beta\gamma}\,\epsilon^*_\alpha v_\beta\, v'_\gamma\,.
\end{aligned} \tag{6}$$

Here the form factors g_i, f_i and k_i are dimensionless functions of $w = v\cdot v'$. At zero recoil ($w = 1$ and $v = v'$) only the g_+, g_{V_1}, and f_{V_1} form factors can contribute, since v' dotted into the polarization ($\epsilon^{*\mu}$ or $\epsilon^{*\mu\alpha}$) vanishes. The variable w is related to the four-momentum transfer squared, $q^2 = (p_B - p_{D^{**}})^2$, as

$$w = v\cdot v' = \frac{m_B^2 + m_{D^{**}}^2 - q^2}{2\, m_B\, m_{D^{**}}}\,. \tag{7}$$

A. Differential decay rates

We define θ as the angle between the charged lepton and the charmed meson in the rest frame of the virtual W boson, i.e., in the center of momentum frame of the lepton pair. It is related to the charged lepton energy via

$$\begin{aligned}
y = 1 - rw - r\sqrt{w^2-1}\,\cos\theta \\
+\,\rho_\ell\,\frac{1 - rw + r\sqrt{w^2-1}\,\cos\theta}{1 - 2rw + r^2}\,,
\end{aligned} \tag{8}$$

where $y = 2E_\ell/m_B$ is the rescaled lepton energy and $\rho_\ell = m_\ell^2/m_B^2$. For the double differential rates in the SM for the $s_l^\pi = \frac{3}{2}^+$ states we obtain

$$\begin{aligned}
&\frac{\mathrm{d}\Gamma_{D_1}}{\mathrm{d}w\,\mathrm{d}\cos\theta} = 3\Gamma_0\, r^3\sqrt{w^2-1}\,\big(1 + r^2 - \rho_\ell - 2rw\big)^2 \\
&\times\Bigg\{\sin^2\theta\left[\frac{\big[f_{V_1}(w-r) + (f_{V_3} + r f_{V_2})(w^2-1)\big]^2}{(1+r^2-2rw)^2} + \rho_\ell\frac{f_{V_1}^2 + \big(2f_A^2 + f_{V_2}^2 + f_{V_3}^2 + 2f_{V_1}f_{V_2} + 2w f_{V_2}f_{V_3}\big)(w^2-1)}{2(1+r^2-2rw)^2}\right]\\
&\quad + (1+\cos^2\theta)\left[\frac{f_{V_1}^2 + f_A^2(w^2-1)}{1+r^2-2rw} + \rho_\ell\frac{[f_{V_1}^2 + (w^2-1)f_{V_3}^2](2w^2 - 1 + r^2 - 2rw)}{2(1+r^2-2rw)^3}\right.\\
&\qquad \left. + \rho_\ell(w^2-1)\frac{2f_{V_1}f_{V_2}(1-r^2) + 4f_{V_1}f_{V_3}(w-r) + f_{V_2}^2(1 - 2rw - r^2 + 2r^2w^2) + 2f_{V_2}f_{V_3}(w - 2r + r^2 w)}{2(1+r^2-2rw)^3}\right]\\
&\quad - 2\cos\theta\,\sqrt{w^2-1}\left[\frac{2f_A f_{V_1}}{1+r^2-2rw} - \rho_\ell\frac{\big[f_{V_1}(w-r) + (f_{V_3} + r f_{V_2})(w^2-1)\big]\big[f_{V_1} + f_{V_2}(1-rw) + f_{V_3}(w-r)\big]}{(1+r^2-2rw)^3}\right]\Bigg\},
\end{aligned} \tag{9}$$

where $r = m_{D^{**}}/m_B$ for each D^{**} state, as appropriate, $\Gamma_0 = G_F^2\,|V_{cb}|^2\, m_B^5/(192\pi^3)$. For $B\to D_2^*\ell\bar{\nu}$ we find

$$\begin{aligned}
&\frac{\mathrm{d}\Gamma_{D_2^*}}{\mathrm{d}w\,\mathrm{d}\cos\theta} = \Gamma_0\, r^3(w^2-1)^{3/2}\,\big(1 + r^2 - \rho_\ell - 2rw\big)^2 \\
&\times\Bigg\{\sin^2\theta\left[\frac{2\big[k_{A_1}(w-r) + (k_{A_3} + r k_{A_2})(w^2-1)\big]^2}{(1+r^2-2rw)^2} + \rho_\ell\frac{3k_{A_1}^2 + \big(3k_V^2 + 2k_{A_2}^2 + 2k_{A_3}^2 + 4k_{A_1}k_{A_2} + 4w k_{A_2}k_{A_3}\big)(w^2-1)}{2(1+r^2-2rw)^2}\right]\\
&\quad + (1+\cos^2\theta)\left[\frac{3}{2}\,\frac{k_{A_1}^2 + k_V^2(w^2-1)}{1+r^2-2rw} + \rho_\ell\frac{[k_{A_1}^2 + (w^2-1)k_{A_3}^2](2w^2 - 1 + r^2 - 2rw)}{(1+r^2-2rw)^3}\right.\\
&\qquad \left. + \rho_\ell(w^2-1)\frac{2k_{A_1}k_{A_2}(1-r^2) + 4k_{A_1}k_{A_3}(w-r) + k_{A_2}^2(1 - 2rw - r^2 + 2r^2w^2) + 2k_{A_2}k_{A_3}(w - 2r + r^2 w)}{(1+r^2-2rw)^3}\right]\\
&\quad - 2\cos\theta\,\sqrt{w^2-1}\left[\frac{3k_V k_{A_1}}{1+r^2-2rw} - 2\rho_\ell\frac{\big[k_{A_1}(w-r) + (k_{A_3} + r k_{A_2})(w^2-1)\big]\big[k_{A_1} + k_{A_2}(1-rw) + k_{A_3}(w-r)\big]}{(1+r^2-2rw)^3}\right]\Bigg\}.
\end{aligned} \tag{10}$$

For the $\frac{1}{2}^+$ D^{**} mesons, the rate for $\mathrm{d}\Gamma_{D_1^*}/\mathrm{d}w\,\mathrm{d}\cos\theta$ is obtained from the D_1 rate above via the replacements

$\{f_A \to g_A,\, f_{V_1} \to g_{V_1},\, f_{V_2} \to g_{V_2},\, f_{V_3} \to g_{V_3}\}$, and for $B \to D_0^* \ell \bar\nu$ we find

$$\begin{aligned}\frac{\mathrm{d}\Gamma_{D_0^*}}{\mathrm{d}w\,\mathrm{d}\cos\theta} &= 3\Gamma_0\, r^3 \sqrt{w^2-1}\big(1-2rw+r^2-\rho_\ell\big)^2 \bigg\{ \sin^2\theta\, \frac{[g_+(1+r)-g_-(1-r)]^2\,(w^2-1)+\rho_\ell[g_+^2(w+1)+g_-^2\,(w-1)]}{(1+r^2-2rw)^2} \\ &\quad + (1+\cos^2\theta)\,\rho_\ell\, \frac{\big[g_+^2(w+1)+g_-^2\,(w-1)\big]\big(w-2r+r^2w\big)-2g_-g_+(1-r^2)(w^2-1)}{(1+r^2-2rw)^3} \\ &\quad - 2\cos\theta\,\rho_\ell\,\sqrt{w^2-1}\,\frac{[g_+(1+r)-g_-(1-r)]\,[g_-(1+r)(w-1)-g_+(1-r)(w+1)]}{(1+r^2-2rw)^3}\bigg\}. \end{aligned} \tag{11}$$

The $\sin^2\theta$ terms are the helicity zero rates, while the $1+\cos^2\theta$ and $\cos\theta$ terms determine the helicity $\lambda=\pm1$ rates. The decay rates for $|\lambda|=1$ vanish for massless leptons at maximal recoil, $w_{\rm max}=(1+r^2-\rho_\tau)/(2r)$, as implied by the $(1-2rw+r^2-\rho_\tau)$ factors.

At zero recoil, the leading contributions to the matrix elements of the weak currents are determined by $f_{V_1}(1)$, $g_{V_1}(1)$, and $g_+(1)$, which are of order $\Lambda_{\rm QCD}/m_{c,b}$. The contributions of other form factors are suppressed by powers of $w-1$. The model independent result is that these numerically significant $\mathcal{O}(\Lambda_{\rm QCD}/m_{c,b})$ effects at $w=1$ are determined in terms of hadron masses and the leading Isgur-Wise function, without dependence on any subleading $\mathcal{O}(\Lambda_{\rm QCD}/m_{c,b})$ Isgur-Wise functions [8]. The results in Eqs. (9)–(11) show that this holds even for $\rho_\ell\neq0$, and treating $\rho_\ell=\mathcal{O}(1)$, since

$$\begin{aligned}\sqrt{6}\,f_{V_1}(w) &= -\big[w^2-1+8\,\varepsilon_c(\bar\Lambda'-\bar\Lambda)\big]\tau(w)+\dots\,, \\ g_+(w) &= -\frac{3}{2}\,(\varepsilon_c+\varepsilon_b)\,(\bar\Lambda^*-\bar\Lambda)\,\zeta(w)+\dots\,, \\ g_{V_1}(w) &= \big[w-1+(\varepsilon_c-3\,\varepsilon_b)\,(\bar\Lambda^*-\bar\Lambda)\big]\zeta(w)+\dots\,, \end{aligned} \tag{12}$$

where $\varepsilon_{c,b}=1/2m_{c,b}$ and the ellipses denote $\mathcal{O}[\varepsilon_{c,b}(w-1)]$, $\mathcal{O}[(w-1)\,\alpha_s]$, and higher order terms. In contrast, Eqs. (A1) – (A4) in Appendix A show that the other form factors depend on subleading Isgur-Wise functions, even at $w=1$. The $B\to D^{**}\tau\bar\nu$ rate and $R(D^{**})$ were previously studied using QCD sum rule calculation of the leading Isgur-Wise function [21].

B. Form factors and approximations

Heavy quark symmetry [7] implies that in the $m_{c,b}\gg\Lambda_{\rm QCD}$ limit the form factors defined in Eqs. (5) and (6) are determined by a single universal Isgur-Wise function, which we denote by $\tau(w)$ and $\zeta(w)$, respectively, for the $\frac{3}{2}^+$ and $\frac{1}{2}^+$ states.[1] In the $m_{c,b}\gg\Lambda_{\rm QCD}$ limit, the contributions of τ and ζ vanish at $w=1$, thus the rates near zero recoil entirely come from $\Lambda_{\rm QCD}/m_{c,b}$ corrections. Some of the $\Lambda_{\rm QCD}/m_{c,b}$ corrections can be expressed in terms of the leading Isgur-Wise function and meson mass splittings [8, 9]. The full expressions are reproduced for completeness in Appendix A. The leading order Isgur-Wise function for the $\frac{3}{2}^+$ states can be parametrized as

$$\tau(w)=\tau(1)\big[1+(w-1)\,\tau'(1)+\dots\big]\,, \tag{13}$$

and $\tau(1)$ can be constrained from the measured $\bar B\to D_1\,\ell\,\bar\nu$ branching fraction. In Ref. [9] the dependence of the predictions was studied as a function of τ', taken to be near -1.5, based on model predictions [22–25]; with more data a fit to all information is preferred.

In any nonrelativistic constituent quark model with spin-orbit independent potential [24, 26] the Isgur-Wise functions for the $s_l^\pi=\frac{3}{2}^+$ and $s_l^\pi=\frac{1}{2}^+$ states are related,

$$\zeta(w)=\frac{w+1}{\sqrt{3}}\,\tau(w)\,. \tag{14}$$

This relation determines the form factor for the broad states from the narrow states' form factor slope and normalization. (See Refs. [27, 28] for exploratory calculations of these Isgur-Wise functions using lattice QCD.)

The form factors at order $\Lambda_{\rm QCD}/m_{c,b}$ depend on several additional functions. The τ_i and ζ_i parameterize corrections to the $b\to c$ current, while η_i and χ_i parameterize matrix elements involving time ordered products of subleading terms in the HQET Lagrangian. Since the range in w is small, for simplicity these functions may be taken to be proportional to the leading Isgur-Wise function. Since the kinetic energy operator does not violate heavy quark spin symmetry, its effects can be absorbed into the leading Isgur-Wise functions by the replacements $\tau\to\tau+\varepsilon_c\,\eta_{\rm ke}^{(c)}+\varepsilon_b\,\eta_{\rm ke}^{(b)}$ and $\zeta\to\zeta+\varepsilon_c\,\chi_{\rm ke}^{(c)}+\varepsilon_b\,\chi_{\rm ke}^{(b)}$.

In what Ref. [9] called Approximation A, the kinematic range, $0\le w-1\lesssim1.3$, is treated as a quantity of order $\Lambda_{\rm QCD}/m_{c,b}$, and the rates are expanded to order ε^2 beyond the $\sqrt{w^2-1}$ phase space factors, where $\varepsilon=\mathcal{O}(w-1)=\mathcal{O}(\Lambda_{\rm QCD}/m_{c,b})$. Its generalization for $\rho_\ell\neq0$ is given in Appendix B. An advantage is that this approach unambiguously truncates the number of fit parameters to a small number; only 5 parameters occur for each of the the $\frac{3}{2}^+$ and $\frac{1}{2}^+$ states, $\{\tau,\,\hat\tau',\,\hat\eta_1,\,\hat\eta_3,\,\hat\eta_b\}$ and $\{\zeta,\,\hat\zeta',\,\hat\chi_1,\,\hat\chi_2,\,\hat\chi_b\}$, respectively. Among these, the first two are the zero-recoil values and slopes of the Isgur-Wise functions, and the latter three are matrix elements

[1] Another often used notation in the literature is $\tau(w)=\sqrt{3}\,\tau_{3/2}(w)$ and $\zeta(w)=2\,\tau_{1/2}(w)$.

of time ordered products involving the chromomagnetic operator. These η-s and χ-s were neglected in Ref. [9].

To study lepton universality, another reason to consider Approximation A is because it would be advantageous both theoretically [6] and experimentally [29] to consider instead of $R(X)$ in Eq. (3), ratios in which the range of q^2 integration is the same in the numerator and the denominator,

$$\widetilde{R}(X) = \frac{\displaystyle\int_{m_\tau^2}^{(m_B-m_X)^2} \frac{\mathrm{d}\Gamma(B\to X\tau\bar\nu)}{\mathrm{d}q^2}\,\mathrm{d}q^2}{\displaystyle\int_{m_\tau^2}^{(m_B-m_X)^2} \frac{\mathrm{d}\Gamma(B\to Xl\bar\nu)}{\mathrm{d}q^2}\,\mathrm{d}q^2}\,. \tag{15}$$

Including the $0 < q^2 < m_\tau^2$ region in the denominator in Eq. (3) dilutes the sensitivity to new physics, and the uncertainties of the form factors increase at larger w (smaller q^2). Taking the average D^{**} mass as near 2.4 GeV, the kinematic range in $B \to D^{**}\tau\bar\nu$ is only about $1 \le w \lesssim 1.2$. Approximation A should work better for this reduced kinematic range, $0 \le w-1 \lesssim 0.2$, than for the total D^{**} rates.

In Approximation B and C the full w dependence known at order $\Lambda_{\rm QCD}/m_{c,b}$ is included. To reduce the number of free parameters, Ref. [9] assumed a linear shape for the leading Isgur-Wise functions, and that the subleading ones have the same shapes. Motivated by the form of the constraints imposed by the equations of motions on the $\Lambda_{\rm QCD}/m_{c,b}$ corrections, two variants were explored,

$$\text{Approx. B}_1: \begin{cases} \frac{3}{2}^+ \text{ states: } \tau_1 = \tau_2 = 0\,, \\ \frac{1}{2}^+ \text{ states: } \zeta_1 = 0\,, \end{cases} \tag{16}$$

$$\text{Approx. B}_2: \begin{cases} \frac{3}{2}^+ \text{ states: } \tau_1 = \bar\Lambda\tau,\ \tau_2 = -\bar\Lambda'\tau\,, \\ \frac{1}{2}^+ \text{ states: } \zeta_1 = \bar\Lambda\zeta\,. \end{cases} \tag{17}$$

In this paper we also study a generalization,

$$\text{Approx. C}: \begin{cases} \frac{3}{2}^+ \text{ states: } \tau_1 = \hat\tau_1\tau,\ \tau_2 = \hat\tau_2\tau\,, \\ \frac{1}{2}^+ \text{ states: } \zeta_1 = \hat\zeta_1\zeta\,, \end{cases} \tag{18}$$

where the normalization of the subleading Isgur-Wise functions is determined from experimental constraints. We also study in Approximation C the impact of not neglecting the chromomagnetic matrix elements. As explained above, this is motivated by the sizable mass splitting, $m_{D_1^*} - m_{D_0^*}$. Note also the large coefficients of η_1 (10 and 12) in the f_{V_2} and f_{V_3} form factors in Eq. (A3).

III. FORM FACTOR FIT

The parameters that occur in the expansions of the form factors can be constrained by the measured semileptonic rates. Belle and *BABAR* measured the total branching fraction of the four D^{**} states and Belle in addition the q^2 distribution of $B \to D_2^* l\bar\nu$ and $B \to D_0 l\bar\nu$ [30, 31]. The measurements were carried out in the $D^{**} \to D^{(*)+}\pi^-$ channels, and to confront the measured branching fractions with decay rate predictions, one needs to account for missing isospin conjugate decay modes and other missing contributions. The missing isospin modes can be accounted for with the factor

$$f_\pi = \frac{\mathcal{B}(D^{**} \to D^{(*)\,0}\,\pi^-)}{\mathcal{B}(D^{**} \to D^{(*)}\pi)} = \frac{2}{3}\,. \tag{19}$$

The measurements of the $B^- \to D_2^{*0}\,l\,\bar\nu$ branching fraction that enter the world average are converted to only account for the $D_2^{*0} \to D^{*+}\pi^-$ decay. To account for the missing $D_2^{*0} \to D^+\pi^-$ decay a correction factor

$$f_{D_2^*} = \frac{\mathcal{B}(D_2^{*0} \to D^{*+}\pi^-)}{\mathcal{B}(D_2^{*0} \to D^+\pi^-)} = 0.65 \pm 0.06\,, \tag{20}$$

from Ref. [32] is applied.

The measurements of the $B^- \to D_1^0\,l\,\bar\nu$ branching fraction do not include contributions of the observed three-body decay of the D_1. This is corrected with a factor

$$f_{D_1} = \frac{\mathcal{B}(D_1^0 \to D^{*+}\pi^-)}{\mathcal{B}(D_1^0 \to D^0\,\pi^+\,\pi^-)} = 2.32 \pm 0.54\,, \tag{21}$$

as calculated from the ratio of nonleptonic $B^+ \to \bar D_1^0\,\pi^+$ decays of Ref. [33]. Assuming no intermediate resonances are present in the three-body decay of a D^{**} meson, one obtains an isospin correction factor of

$$f_{\pi\pi} = \frac{\mathcal{B}(D^{**} \to D^{(*)-}\,\pi^+\,\pi^-)}{\mathcal{B}(D^{**} \to D^{(*)}\pi\pi)} = \frac{9}{16}\,. \tag{22}$$

If the three-body final state of a D^{**} meson is reached through resonances, i.e., via $f_0(500) \to \pi\pi$ or $\rho \to \pi\pi$ decays, this factor is either 2/3 or 1/3, respectively. In what follows we adapt the prescription proposed in Ref. [34] and apply an average correction factor

$$f_{\pi\pi} = \frac{1}{2} \pm \frac{1}{6}\,, \tag{23}$$

with an uncertainty spanning all three scenarios. After these corrections we make the explicit assumption that

$$\begin{aligned} \mathcal{B}(\bar D_2^* \to \bar D\,\pi) + \mathcal{B}(\bar D_2^* \to \bar D^*\,\pi) &= 1\,, \\ \mathcal{B}(\bar D_1 \to \bar D^*\,\pi) + \mathcal{B}(\bar D_1 \to \bar D\,\pi\,\pi) &= 1\,, \\ \mathcal{B}(\bar D_1^* \to \bar D^*\,\pi) &= 1\,, \\ \mathcal{B}(\bar D_0^* \to \bar D\,\pi) &= 1\,, \end{aligned} \tag{24}$$

and then all semileptonic rates and differential rates can be related. Table V summarizes the corrected total branching fractions. The summed $B \to D^{(*)}\pi\pi\,l\,\bar\nu_\ell$ contributions can be compared with the measurement of Ref. [34]. The reported semi-inclusive $B^+ \to D\,\pi\,\pi\,l\,\bar\nu_\ell$ rates can be nearly accommodated by the expected $D_1 \to D\,\pi\,\pi$ contribution

$$\begin{aligned} &\mathcal{B}(B^+ \to \bar D^0\,\pi\,\pi\,l\,\bar\nu) - \mathcal{B}(B^+ \to \bar D_1^0(\to \bar D^0\,\pi\,\pi)\,l\,\bar\nu) \\ &\qquad = (0.06 \pm 0.16) \times 10^{-2}\,. \end{aligned} \tag{25}$$

Decay mode	Branching fraction
$B^+ \to \bar{D}_2^{*0}\, l\, \bar{\nu}$	$(0.30 \pm 0.04) \times 10^{-2}$
$B^+ \to \bar{D}_1^{0}\, l\, \bar{\nu}$	$(0.67 \pm 0.05) \times 10^{-2}$
$B^+ \to \bar{D}_1^{*0}\, l\, \bar{\nu}$	$(0.20 \pm 0.05) \times 10^{-2}$
$B^+ \to \bar{D}_0^{*0}\, l\, \bar{\nu}$	$(0.44 \pm 0.08) \times 10^{-2}$

TABLE V. The corrected world averages of the semileptonic decay rates into excited charmed mesons [32]. The corrections described in the text involve factors to account for missing isospin conjugate modes and observed three-body decays.

w	$B^+ \to \bar{D}_2^{*0}\, l\, \bar{\nu}$	$B^+ \to \bar{D}_0^{*0}\, l\, \bar{\nu}$
$1.00 - 1.08$	0.06 ± 0.02	0.05 ± 0.02
$1.08 - 1.16$	0.30 ± 0.05	0.02 ± 0.05
$1.16 - 1.24$	0.38 ± 0.03	0.30 ± 0.08
$1.24 - 1.32$	0.26 ± 0.06	0.30 ± 0.09
$1.32 - 1.40$	—	0.33 ± 0.13

TABLE VI. The normalized differential decay rates for $B^+ \to \bar{D}_2^{*0}\, l\, \bar{\nu}$ and $B^+ \to \bar{D}_0^{*0}\, l\, \bar{\nu}$ as functions of w [30].

Decays of the type $\bar{D}^{**} \to \bar{D}^* \pi\pi$ have been searched for [35], but no sizable contribution that could explain the large reported $\mathcal{B}(B^+ \to \bar{D}^{*0}\, \pi\, \pi\, l\, \bar{\nu})$ branching fraction [34] have been observed. It seems likely that such contributions originate either from higher excitations or nonresonant semileptonic decays, which would not affect the predictions discussed in this paper. Table VI summarizes the measured normalized differential decay rates of $B^+ \to \bar{D}_2^{*0}\, l\, \bar{\nu}$ and $B^+ \to \bar{D}_0^{*0}\, l\, \bar{\nu}$ as functions of w.

Additional constraints on the form factors at maximal recoil come from nonleptonic $B^0 \to D^{**-}\, \pi^+$ decays. Factorization should be a good approximation for B decays into charmed mesons and a charged pion [36, 37]. Contributions that violate factorization are suppressed by $\Lambda_{\rm QCD}$ divided by the energy of the pion in the B restframe or by $\alpha_s(m_Q)$. Neglecting the pion mass, the two-body decay rate, Γ_π, is related to the differential decay rate $\mathrm{d}\Gamma_{\rm sl}/\mathrm{d}w$ at maximal recoil for the analogous semileptonic decay (with the π replaced by the $l\bar{\nu}$ pair)

$$\Gamma_\pi = \frac{3\pi^2\, |V_{ud}|^2\, C^2 f_\pi^2}{m_B^2\, r} \left(\frac{\mathrm{d}\Gamma_{\rm sl}}{\mathrm{d}w} \right)_{w_{\rm max}} . \qquad (26)$$

Here C is a combination of Wilson coefficients of four-quark operators and numerically $|V_{ud}|\, C$ is very close to unity. Table VII summarizes the measured nonleptonic rates, after all correction factors for missing isospin and three-body decays are applied. The smallness of $\mathcal{B}(B^0 \to D_0^{*-}\pi^+)$ is puzzling [38, 39], and measurements using the full *BABAR* and Belle data sets would be worthwhile. It would also be interesting to measure in Belle II the color suppressed $B^0 \to D^{**0}\pi^0$ rates, for which SCET predicts $\mathcal{B}(B^0 \to D_2^{*0}\pi^0)/\mathcal{B}(B^0 \to D_1^0\pi^0) = 1$ [40].

The narrow and broad states semileptonic and narrow states nonleptonic inputs are analyzed to construct a likelihood to determine the form factor parameters of Approximation A, B and C. This is done separately for the narrow $\frac{3}{2}^+$ and broad $\frac{1}{2}^+$ states.

Decay mode	Branching fraction
$B^0 \to D_2^{*-}\pi^+$	$(0.59 \pm 0.13) \times 10^{-3}$
$B^0 \to D_1^{-}\pi^+$	$(0.75 \pm 0.16) \times 10^{-3}$
$B^0 \to D_0^{*-}\pi^+$	$(0.09 \pm 0.05) \times 10^{-3}$

TABLE VII. World averages of nonleptonic $B^0 \to D^{**-}\pi^+$ branching ratios [32], after the corrections described in the text are applied.

A. Approximation A

The main parameters that determine Approximation A are the normalization and slope of the leading Isgur-Wise function for the narrow and broad states, $\{\tau(1), \tau'\}$ and $\{\zeta(1), \zeta'\}$. In addition, the inclusion of one or two subleading Isgur-Wise functions parameterizing chromomagnetic contributions is explored. These are extracted by building a likelihood using experimental quantities, which are less sensitive to the absence of subleading Isgur-Wise functions from matrix elements of subleading currents in Approximation A (see, Appendix B). These are the semileptonic branching fractions to the narrow $\frac{3}{2}^+$ states and the nonleptonic $B^0 \to D_2^{*-}\pi^+$ branching fraction. The constraint from the nonleptonic $B^0 \to D_1^{-}\pi^+$ branching fraction is not included in the fit, as the semileptonic rate to D_1 near $q^2 = m_\pi^2$ receives large corrections from subleading Isgur-Wise functions that do not enter Approximation A. Such contributions only mildly affect the total branching fraction. The analysis of the broad $\frac{1}{2}^+$ states uses the measured semileptonic branching fractions only.

Figure 1 (top left) shows the 68% and 95% confidence regions for the normalization and slope of the leading Isgur-Wise function for the narrow $\frac{3}{2}^+$ states. The scenarios explored are: no chromomagnetic contributions, one chromomagnetic term (either η_1, η_3, or η_b; note that η_b and η_1 are degenerate in Approximation A), or two chromomagnetic terms (either η_1 or η_b with η_3) marginalized. Table VIII summarizes the best fit points. There is no sensitivity to disentangle the different chromomagnetic contributions, and the fitted values are compatible with zero. The extracted value for the slope of the leading Isgur-Wise function is compatible with the -1.5 quark model prediction in all scenarios.

Figure 1 (top right) shows the 68% and 95% confidence regions for the normalization and slope of the leading Isgur-Wise function for the broad $\frac{1}{2}^+$ states. The available experimental information only loosely constrains the form factor parameters and introducing one chromomagnetic contribution results only in marginal shifts of the

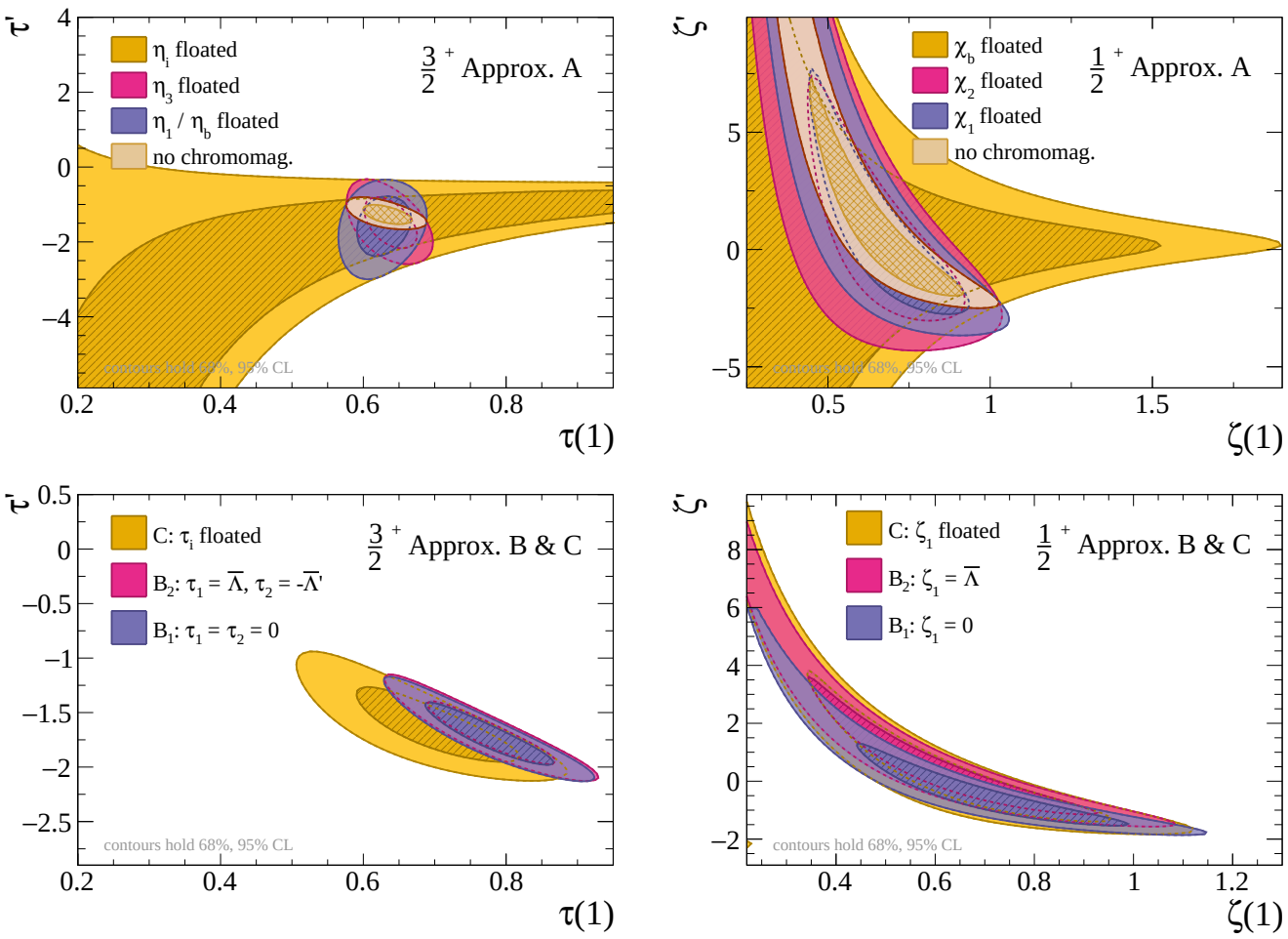

FIG. 1. The allowed 68% and 95% regions for $\tau(1)$ and τ' or $\zeta(1)$ and ζ', respectively, are shown for the narrow $\frac{3}{2}^+$ (left) and broad $\frac{1}{2}^+$ states (right) for Approximation A (top) and Approximation B (bottom).

extracted normalization and slope of the leading Isgur-Wise function. The extracted value for the slope of the leading Isgur-Wise function is compatible with quark model predictions of -1.0 and the obtained chromomagnetic contributions are compatible with zero. Table VIII summarizes the extracted best fit points. Table IX summarizes the χ^2 values of all fits and the agreement of the best fit points with the experimental input is good for the $\frac{3}{2}^+$ states and $\frac{1}{2}^+$ states for all scenarios.

Using the extracted values of the normalization and slope of the leading Isgur-Wise function, and possible chromomagnetic contributions, the ratio of semi-tauonic and semileptonic rates can be predicted. Including chromomagnetic contributions change the central values of the predicted ratios only marginally, but increase the uncertainties. Using the fitted values, we predict

$$R(D_2^*) = 0.06 \pm 0.01\,, \qquad \widetilde{R}(D_2^*) = 0.14 \pm 0.01\,,$$
$$R(D_1) = 0.06 \pm 0.01\,, \qquad \widetilde{R}(D_1) = 0.17 \pm 0.02\,,$$
$$R(D_1^*) = 0.06 \pm 0.01\,, \qquad \widetilde{R}(D_1^*) = 0.17 \pm 0.02\,,$$

	$\tau(1)$	τ'	η_i
—	0.63 ± 0.02	-1.29 ± 0.17	—
η_1	0.63 ± 0.02	-1.53 ± 0.52	-0.10 ± 0.19
η_3	0.64 ± 0.02	-1.50 ± 0.45	0.14 ± 0.29
η_b	0.63 ± 0.02	-1.53 ± 0.52	0.67 ± 1.32

	$\zeta(1)$	ζ'	χ_i
—	0.72 ± 0.15	-0.30 ± 1.81	—
χ_1	0.73 ± 0.15	-0.53 ± 2.16	0.03 ± 0.15
χ_2	0.72 ± 0.15	-0.54 ± 2.22	-0.05 ± 0.30

TABLE VIII. The best fit points of the Approximation A fits, with and without chromomagnetic contributions for the narrow $\frac{3}{2}^+$ (above) and broad $\frac{1}{2}^+$ (below) states.

$$R(D_0) = 0.07 \pm 0.03\,, \qquad \widetilde{R}(D_0) = 0.22 \pm 0.04\,, \quad (27)$$

and for the ratio of the sum of all four D^{**} modes,

$$R(D^{**}) = 0.061 \pm 0.006\,. \quad (28)$$

	χ^2 / ndf	Prob.
—	2.8 / 5	0.73
η_1	2.5 / 4	0.64
η_3	2.5 / 4	0.64
η_b	2.5 / 4	0.64

	χ^2 / ndf	Prob.
—	8.7 / 6	0.19
χ_1	8.7 / 5	0.12
χ_2	8.7 / 5	0.12

TABLE IX. The χ^2 values and fit probabilities for the Approximation A fits for the narrow $\frac{3}{2}^+$ (left) and broad $\frac{1}{2}^+$ (right) states.

The uncertainties are from the fit to the experimental information and also contain the impact from possible chromomagnetic contributions. In Approximation A, the predictions for $\widetilde{R}(D^{**})$ are more precise and more reliable than for $R(D^{**})$, as the w range is smaller. However, the experimental input to make full use of this is not available yet, as partial branching fractions with a w cut would be needed. Then the parameters in Approximation A could be determined just from the $q^2 > m_\tau^2$ part of phase space, resulting in better precision for these predictions.

The obtained values can be compared to the prediction of the LLSW model. As input we re-fit the normalization of the leading Isgur-Wise function $\tau(1) = 0.64$ using the averaged semileptonic D_1 branching fraction from Table V, and use

$$\zeta(1) = \frac{2}{\sqrt{3}}\,\tau(1)\,, \qquad \zeta' = \tau' + \frac{1}{2}\,, \tag{29}$$

to relate the narrow $\frac{3}{2}^+$ and broad $\frac{1}{2}^+$ Isgur-Wise functions. For the slope we use $\hat\tau' = -1.5$ discussed in Section II B based on model predictions. We find

$$\begin{aligned} R(D_2^*) &= 0.06\,, \qquad \widetilde{R}(D_2^*) = 0.15\,, \\ R(D_1) &= 0.06\,, \qquad \widetilde{R}(D_1) = 0.17\,, \\ R(D_1^*) &= 0.06\,, \qquad \widetilde{R}(D_1^*) = 0.17\,, \\ R(D_0) &= 0.08\,, \qquad \widetilde{R}(D_0) = 0.23\,, \end{aligned} \tag{30}$$

and for the ratio of the sum of all four D^{**} modes,

$$R(D^{**}) = 0.064\,, \tag{31}$$

which are in excellent agreement with Eqs. (27) and (28).

B. Approximation B and C

The parameters of interest for Approximation B are the normalization and slope of the leading Isgur-Wise function, and the normalizations of the subleading Isgur-Wise functions, τ_1, τ_2 or ζ_1 (see Section II B). These parameters are again extracted separately for the broad and narrow states using a simultaneous analysis of all semileptonic and nonleptonic branching fractions. In addition, Approximations B_1 and B_2 are explored, with the normalizations fixed.

Figure 1 (bottom left) shows the 68% and 95% confidence regions for $\tau(1)$ and τ' for the narrow $\frac{3}{2}^+$ states. All three fit scenarios are in good agreement for the normalization and slope of the leading Isgur-Wise function. Table X summarizes the best fit points and the obtained slope is compatible with the quark model predictions used in Ref. [9]. Introducing the normalizations of the subleading Isgur-Wise functions as free parameters, pulls them outside the interval covered by Approximations B_1 and B_2. This is interesting, as in many experimental analyses the difference between Approximations B_1 and B_2 is used as a measure of the uncertainties associated with D^{**} contributions. The Approximation C parameter correlations for $\{\tau(1), \tau', \tau_1, \tau_2\}$. are

$$C_{\frac{3}{2}^+} = \begin{pmatrix} 1 & -0.83 & 0.66 & -0.63 \\ -0.83 & 1 & -0.27 & 0.20 \\ 0.66 & -0.27 & 1 & -0.93 \\ -0.63 & 0.20 & -0.93 & 1 \end{pmatrix}. \tag{32}$$

Figure 1 (bottom right) shows the 68% and 95% confidence regions for $\zeta(1)$ and ζ' for the broad $\frac{1}{2}^+$ states. There is good consistency of the normalizations and slopes of the leading Isgur-Wise function, and the results for all three fits are listed in Table X. The normalization of the subleading Isgur-Wise function, ζ_1, is again outside the interval covered by Approximations B_1 and B_2. Table XI summarizes the compatibility of the best fit points, and the agreement is fair, with the exception of the Approximation B_2 fit for the narrow $\frac{3}{2}^+$ states. The Approximation C parameter correlation for $\{\zeta(1), \zeta', \zeta_1\}$ are

$$C_{\frac{1}{2}^+} = \begin{pmatrix} 1 & -0.95 & -0.35 \\ -0.95 & 1 & 0.51 \\ -0.35 & 0.51 & 1 \end{pmatrix}. \tag{33}$$

Using the fit results, with the normalizations of the subleading Isgur-Wise functions floated, in Approxima-

	$\tau(1)$	τ'	τ_1	τ_2
B_1	0.78 ± 0.06	-1.7 ± 0.2	0	0
B_2	0.78 ± 0.06	-1.7 ± 0.2	0.40	-0.80
C	0.71 ± 0.07	-1.6 ± 0.2	-0.5 ± 0.3	2.9 ± 1.6

	$\zeta(1)$	ζ'	ζ_1
B_1	0.73 ± 0.18	-0.7 ± 0.8	0
B_2	0.66 ± 0.19	0 ± 1.1	0.4
C	0.68 ± 0.20	-0.2 ± 1.2	0.3 ± 0.3

TABLE X. The best fit points of the Approximation B and C fits for the narrow $\frac{3}{2}^+$ (above) and broad $\frac{1}{2}^+$ (below) states.

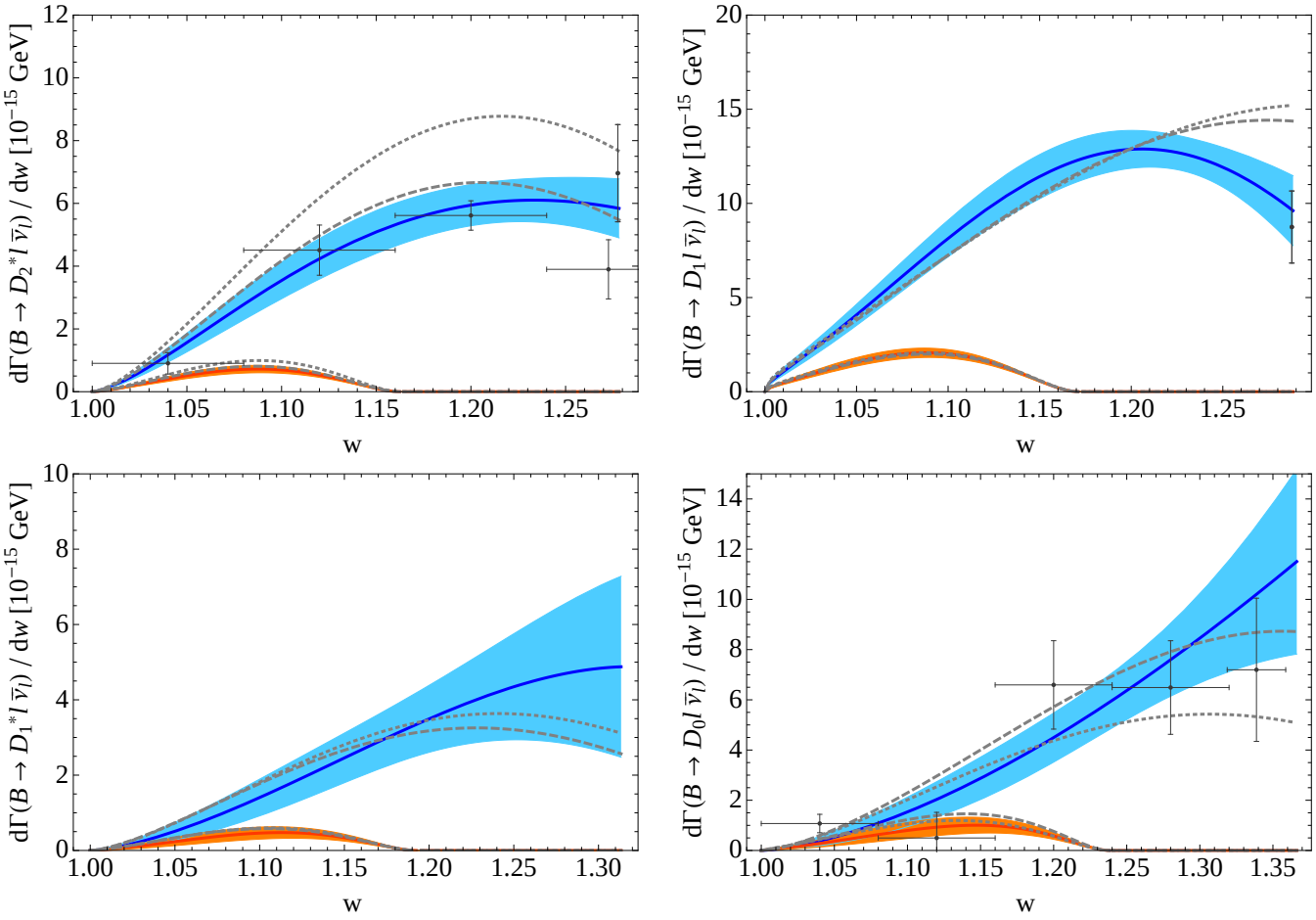

FIG. 2. The colored bands show the allowed 68% regions for $m_\ell = 0$ (blue) and $m_\ell = m_\tau$ (orange) for the differential decay rates in Approximation C. The dashed (dotted) curves show the predictions of Ref. [9] for Approximations B_1 (B_2). The data points correspond to the differential semileptonic or nonleptonic branching fraction measurements described in the text.

tion C we obtain

$$\begin{aligned} R(D_2^*) &= 0.07 \pm 0.01\,, & \widetilde{R}(D_2^*) &= 0.17 \pm 0.01\,, \\ R(D_1) &= 0.10 \pm 0.01\,, & \widetilde{R}(D_1) &= 0.20 \pm 0.01\,, \\ R(D_1^*) &= 0.06 \pm 0.02\,, & \widetilde{R}(D_1^*) &= 0.18 \pm 0.02\,, \\ R(D_0) &= 0.08 \pm 0.03\,, & \widetilde{R}(D_0) &= 0.25 \pm 0.03\,, \end{aligned} \tag{34}$$

and for the ratio for the sum over all four D^{**} states,

$$R(D^{**}) = 0.085 \pm 0.010\,. \tag{35}$$

	χ^2 / ndf	Prob.
B_1	6.1/6	0.42
B_2	11.6/6	0.07
C	2.4/4	0.66

	χ^2 / ndf	Prob.
B_1	10.1/5	0.07
B_2	9.2/5	0.10
C	9.1/4	0.06

TABLE XI. The χ^2 values and fit probabilities for the Approximation B and C fits for the narrow $\frac{3}{2}^+$ (left) and broad $\frac{1}{2}^+$ states (right).

These values can be compared with the LLSW prediction, including the lepton mass effects in Eqs. (9), (10), and (11). Using Eq. (13) for the Isgur-Wise functions for the $\frac{3}{2}^+$ states, and the model prediction in Eq. (14) to relate it to the $\frac{1}{2}^+$ states, we find in Approximation B_1 and B_2, respectively,

$$\begin{aligned} R(D_2^*) &= \{0.072,\, 0.068\}, & \widetilde{R}(D_2^*) &= \{0.159,\, 0.158\}, \\ R(D_1) &= \{0.096,\, 0.099\}, & \widetilde{R}(D_1) &= \{0.221,\, 0.231\}, \\ R(D_1^*) &= \{0.092,\, 0.083\}, & \widetilde{R}(D_1^*) &= \{0.200,\, 0.196\}, \\ R(D_0) &= \{0.107,\, 0.118\}, & \widetilde{R}(D_0) &= \{0.272,\, 0.275\}, \end{aligned} \tag{36}$$

and for the sum of the four D^{**} states,

$$R(D^{**}) = \{0.0949,\, 0.0946\}\,. \tag{37}$$

The ranges spanned by these Approximation B_1 and B_2 results do not necessarily give conservative estimates of the uncertainties. These ratios, however, are in good agreement with Eqs. (34) and (35).

Of the mass parameters, $\bar\Lambda$ has substantially bigger uncertainty than $\bar\Lambda' - \bar\Lambda$ or $\bar\Lambda^* - \bar\Lambda$. Varying $\bar\Lambda$ by $\pm 50\,\mathrm{MeV}$ while keeping the differences fixed has a negligible impact compared to other uncertainties included. This is consistent with the fact that in Approximation A the only dependence on $\bar\Lambda$ is via $\bar\Lambda' - \bar\Lambda$ and $\bar\Lambda^* - \bar\Lambda$.

Figure 2 shows the differential decay rates of the Approximation C fits as functions of w for $m_\ell = 0$ and $m_\ell = m_\tau$, with the corresponding 68% uncertainty bands. The LLSW model prediction is also shown for the differential decay rates: the dashed (dotted) curves show Approximation B_1 (B_2) and the normalization of the leading Isgur-Wise function was determined using the averaged semileptonic D_1 branching fraction, which gives $\tau(1) = 0.80$. The Approximation C fit using the full differential semileptonic and nonleptonic information constrain the shape stronger than the LLSW model, which only uses the D_1 rate information.

We also explore in Approximation C the impact of additional chromomagnetic contributions. The available experimental information does not allow to disentangle subleading Isgur-Wise function contributions from chromomagnetic terms. Figure 3 shows the dependence of $R(D^{**})$ on one of the chromomagnetic contributions at a time. For the narrow $\frac{3}{2}^+$ states the only strong dependence comes from η_1. This originates from large factors in the rate expressions, and if introduced as an additional free parameter in the Approximation C fit, its size is constrained to be about ± 200 MeV, but it is also strongly correlated to other subleading Isgur-Wise function normalizations. For the broad $\frac{1}{2}^+$ states the strongest dependence comes from χ_1. If introduced as an additional free parameter in the Approximation C fit, its size is constrained to be about ± 100 MeV.

To account for these subleading Isgur-Wise functions parameterizing chromoagnetic effects, we can recalculate the ratios of semi-tauonic and semileptonic rates by introducing an additional uncertainty of ± 200 MeV and ± 100 MeV on η_1 and χ_1, respectively. We thus obtain

$$\begin{aligned}
R(D_2^*) &= 0.07 \pm 0.01\,, \qquad & \widetilde R(D_2^*) &= 0.17 \pm 0.01\,,\\
R(D_1) &= 0.10 \pm 0.02\,, \qquad & \widetilde R(D_1) &= 0.20 \pm 0.02\,,\\
R(D_1^*) &= 0.06 \pm 0.02\,, \qquad & \widetilde R(D_1^*) &= 0.18 \pm 0.02\,,\\
R(D_0) &= 0.08 \pm 0.04\,, \qquad & \widetilde R(D_0) &= 0.25 \pm 0.06\,, \qquad (38)
\end{aligned}$$

and for the ratio of the sum over all four D^{**} states,

$$R(D^{**}) = 0.085 \pm 0.012\,. \qquad (39)$$

These uncertainties are not much greater than those in Eqs. (34) and (35).

IV. $B_s \to D_s^{**}\ell\,\bar\nu$ DECAYS

An important difference between $B \to D^{**}\ell\bar\nu$ and $B_s \to D_s^{**}\ell\bar\nu$ is that the two lightest excited D_s states observed are fairly narrow. They are lighter than the $m_{D^{(*)}} + m_K$ mass thresholds, so they can only decay to $D_s^{(*)}\pi$, which violate isospin (if these are the D_s^{**} isosinglet $s_l^{\pi_l} = \frac{1}{2}^+$ orbitally excited states). Due to these narrow widths, semi-tauonic B_s decay to the spin-zero meson, $B_s \to D_{s0}^*\tau\bar\nu$, may be easier to measure than $B \to D_0^*\tau\bar\nu$, and may provide good sensitivity to possible scalar interactions from new physics.[2] Table XII summarizes the relevant masses and widths.

While the $s_l^{\pi_l} = \frac{3}{2}^+$ doublets in both the D_s^{**} and B_s^{**} cases have masses "as expected", about 100 MeV above their non-strange counterparts, the masses of the $s_l^{\pi_l} = \frac{1}{2}^+$ doublet of D_s^{**} states are surprisingly close to their non-strange counterparts. (Which is why the discovery of the D_{s0}^* [41] was such a surprise.) This unexpected spectrum makes the analysis in this Section more uncertain than in the previous ones.

It is possible that interpreting the D_{s0}^* and D_{s1}^* as the lightest orbitally excited states is oversimplified (and this is what our description assumes), and we have higher confidence that our description of the decays to the $s_l^{\pi_l} = \frac{3}{2}^+$ D_{s1} and D_{s2}^* states should be reliable. The first exploratory lattice QCD studies that obtain the D_{s0}^* and D_{s1}^* masses in agreement with data appeared only recently [42]. To be more specific, assuming that the D_{s0}^* is the lightest orbitally excited D_s state, theoretical predictions for $\mathcal{B}(D_{s0} \to D_s^*\gamma)/\mathcal{B}(D_{s0} \to D_s\pi)$ tend to be above [43–45] the CLEO upper bound, $\mathcal{B}(D_{s0} \to D_s^*\gamma)/\mathcal{B}(D_{s0} \to D_s\pi) < 0.059$ (90% CL) [46]. The $D^{(*)}K$ molecular picture of these states also faces challenges, e.g., the lack of observed isospin partners [47]. It is possible that the correct description is a mixture of these. However, given that the CLEO bound [46] was obtained with 13.5/fb data, and the Belle bound on the above ratio < 0.18 (90% CL) [48] used 87/fb, while the *BABAR* result < 0.16 (95% CL) [49] used 232/fb, remeasuring $\mathcal{B}(D_{s0} \to D_s^*\gamma)/\mathcal{B}(D_{s0} \to D_s\pi)$ using the full *BABAR* and Belle data would be desirable.

Another piece of data is that the mass splittings within each heavy quark spin symmetry doublets appear to be consistent with nominal $SU(3)$ breaking between the strange and non-strange states. This supports the fact that the mass splittings in the $s_l^{\pi_l} = \frac{1}{2}^+$ doublets are comparable to $m_{D^*} - m_D \simeq m_{D_s^*} - m_{D_s}$, unlike what LLSW considered based on the data in 1997.

For the HQET mass parameters we use $\bar\Lambda_s = \bar\Lambda + 90\,\mathrm{MeV}$, motivated by $\overline{m}_{B_s} - \overline{m}_B$. We also estimate $\bar\Lambda_s' - \bar\Lambda_s = 0.41\,\mathrm{GeV}$ using Eq. (1.10) in Ref. [9]. For $\bar\Lambda_s' - \bar\Lambda_s^* = 0.13\,\mathrm{GeV}$ from the $(2555 - 2425)\,\mathrm{MeV}$ difference in Table XIII. (These values are also shown in Table IV.).

Using $SU(3)$ flavor symmetry to relate the $B \to D^{**}\ell\bar\nu$ decay parameters to $B_s \to D_s^{**}\ell\bar\nu$, in Approximation C

[2] We thank Marcello Rotondo for drawing our attention to this.

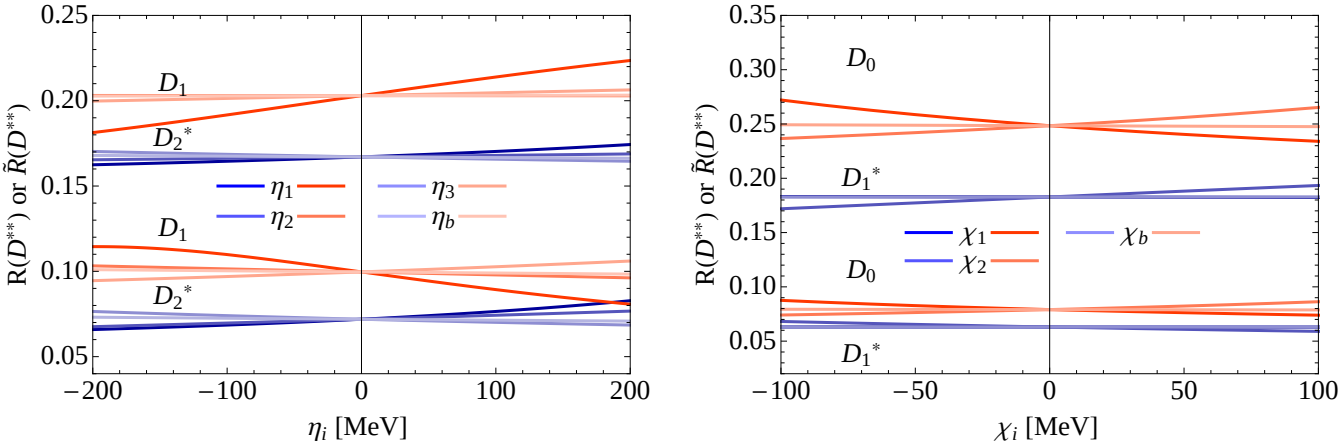

FIG. 3. The impact of chromomagnetic contributions η_i and χ_i on the exclusive ratios $R(D^{**})$ (below 0.15) and $\widetilde{R}(D^{**})$ (above 0.15). For the leading and subleading Isgur-Wise functions the best fit parameters of Approximation C (without including chromomagnetic terms) are used. The explored range is motivated by the experimental constraints of η_1 and χ_1 (see the text).

Particle	$s_l^{\pi_l}$	J^P	m (MeV)	Γ (MeV)
D_{s0}^*	$\frac{1}{2}^+$	0^+	2318	< 4
D_{s1}^*	$\frac{1}{2}^+$	1^+	2460	< 4
D_{s1}	$\frac{3}{2}^+$	1^+	2535	1
D_{s2}^*	$\frac{3}{2}^+$	2^+	2567	17
B_{s1}	$\frac{3}{2}^+$	1^+	5829	1
B_{s2}^*	$\frac{3}{2}^+$	2^+	5840	1

TABLE XII. Same as Table I, but for D_s mesons. For the $\frac{3}{2}^+$ states we averaged the PDG with a recent LHCb measurement [50] not included in the PDG.

$s_l^{\pi_l}$	Particles	$\overline{m}$ (MeV)	Particles	$\overline{m}$ (MeV)
$\frac{1}{2}^-$	D_s, D_s^*	2076	B_s, B_s^*	5403
$\frac{1}{2}^+$	D_{s0}^*, D_{s1}^*	2425	B_{s0}^*, B_{s1}^*	—
$\frac{3}{2}^+$	D_{s1}, D_{s2}^*	2555	B_{s1}, B_{s2}^*	5836

TABLE XIII. Same as Table III, but for D_s and B_s mesons.

we predict for the ratios of the τ to light-lepton rates

$$\begin{aligned} R(D_{s2}^*) &= 0.07 \pm 0.01\,, & \widetilde{R}(D_{s2}^*) &= 0.16 \pm 0.01\,,\\ R(D_{s1}) &= 0.09 \pm 0.02\,, & \widetilde{R}(D_{s1}) &= 0.20 \pm 0.02\,,\\ R(D_{s1}^*) &= 0.07 \pm 0.03\,, & \widetilde{R}(D_{s1}^*) &= 0.20 \pm 0.02\,,\\ R(D_{s0}^*) &= 0.09 \pm 0.04\,, & \widetilde{R}(D_{s0}^*) &= 0.26 \pm 0.05\,. \end{aligned} \tag{40}$$

This is the analog of Eq. (38), with increased uncertainties to account for the impact of additional chromomagnetic contributions, which cannot be constrained well yet. These predictions will improve when more data is available on $B \to D^{**}\ell\bar{\nu}$, or $B_s \to D_s^{**}\ell\bar{\nu}$, or related $B_{(s)} \to D_{(s)}^{**}\pi$ rates.

V. $B \to D^{**}\tau\,\bar{\nu}$ AND SCALAR INTERACTIONS

To illustrate the complementary sensitivities to new physics, in this section we explore the impacts of possible scalar interactions on $R(D^{**})$. We consider the effective Hamiltonian,

$$\begin{aligned} \mathcal{H} = \frac{4G_F}{\sqrt{2}}\,V_{cb}\,\big[&(\bar{c}\gamma_\mu P_L b)\,(\bar{\tau}\gamma^\mu P_L \nu) \\ &+ S_L(\bar{c}P_L b)\,(\bar{\tau}P_L\nu) + S_R(\bar{c}P_R b)\,(\bar{\tau}P_L\nu)\big]. \end{aligned} \tag{41}$$

This notation follows Ref. [2], although without specifying details of the underlying model, one may expect $S_{L,R} = \mathcal{O}[m_W^2/(|V_{cb}|\Lambda^2)]$. For simplicity, we consider two scenarios. (i) In the type-II 2HDM, $S_L = 0$ and $S_R = -m_b\,m_\tau\tan^2\beta/m_{H^\pm}^2$. This scenario is motivated by being the Higgs sector of the MSSM; it does not give a good fit to the current data, however, the central values of $R(D^{(*)})$ may change in a way that this conclusion is altered, but a robust deviation from the SM remains. (ii) In another scenario that we consider, $S_L + S_R = 0.25$ and we study the dependence of $R(D^{**})$ on $S_L - S_R$. This is motivated by giving a good fit the current data, and can arise, e.g., in other extensions of the Higgs sector.

While Eq. (41) is natural to write in terms of left- and right-handed operators, the hadronic matrix elements are simpler to address in terms of the scalar $(\bar{c}b)$ and pseudoscalar $(\bar{c}\gamma_5 b)$ currents. In particular,

$$\begin{aligned} \langle D_0^*|\bar{c}b|B\rangle &= 0\,, & \langle D_1^*|\bar{c}\gamma_5 b|B\rangle &= 0\,,\\ \langle D_2^*|\bar{c}b|B\rangle &= 0\,, & \langle D_1|\bar{c}\gamma_5 b|B\rangle &= 0\,, \end{aligned} \tag{42}$$

whereas $\langle D^*|\bar{c}b|B\rangle = 0$ and $\langle D|\bar{c}\gamma_5 b|B\rangle = 0$ for the D and D^*. The non-vanishing (pseudo)scalar matrix elements can be related to those of the SM currents via

$$\begin{aligned} \langle X|\bar{c}\gamma_5 b|B\rangle &= \frac{-q^\mu}{m_b + m_c}\,\langle X|\bar{c}\gamma_\mu\gamma_5 b|B\rangle\,,\\ \langle X|\bar{c}b|B\rangle &= \frac{q^\mu}{m_b - m_c}\,\langle X|\bar{c}\gamma_\mu b|B\rangle\,. \end{aligned} \tag{43}$$

The charged Higgs contribution is simplest to include by writing the rate in terms of a helicity decomposition. The differential decay rate with its full lepton mass dependence can be written as

$$\frac{\mathrm{d}\Gamma(B\to D^{**}\ell\,\bar\nu)}{\mathrm{d}q^2} = \frac{G_F^2\,|V_{cb}|^2\,|\vec p\,'|\,q^2}{96\pi^3\,m_B^2}\left(1-\frac{m_\ell^2}{q^2}\right)^2 \times\left[\sum_{k=\pm,0,t} H_k^2\left(1+\frac{m_\ell^2}{2q^2}\right)+\frac{3}{2}\frac{m_\ell^2}{q^2}H_t^2\right], \quad (44)$$

with the helicity amplitudes $H_{k=\pm,0,t}$ (we use the notation of Ref. [51]). Here $|\vec p\,'|$ is the magnitude of the three-momentum of the D^{**}. It is related to q^2 as

$$|\vec p\,'|^2 = \left(\frac{m_B^2+m_{D^{**}}^2-q^2}{2m_B}\right)^2 - m_{D^{**}}^2 = m_{D^{**}}^2(w^2-1)\,. \quad (45)$$

Setting $m_\ell = 0$, one recovers the expression

$$\frac{\mathrm{d}\Gamma(B\to D^{**}\ell\bar\nu)}{\mathrm{d}q^2} = \frac{G_F^2\,|V_{cb}|^2\,|\vec p\,'|\,q^2}{96\pi^3\,m_B^2}\sum_{k=\pm,0,t} H_k^2\,, \quad (46)$$

which is an excellent approximation for $l = e, \mu$.

The contributions of the scalar operators can be included by replacing H_t according to

$$H_t \to H_t^{\rm SM}\left[1+(S_R\pm S_L)\,\frac{q^2}{m_\tau(m_b\mp m_c)}\right], \quad (47)$$

where the upper signs are for the final states D, D_1^* and D_1, and the lower signs are for D^*, D_0^*, and D_2^*. The helicity amplitudes $H_{\pm,0,t}$ are related to the form factors defined in Eqs. (5) and (6), and the full expressions for all four D^{**} states are given in Appendix C.

The upper plot in Fig. 4 shows the ratios of τ to light-lepton rates as functions of $\tan\beta/m_{H^\pm}$ for the four D^{**} states and for comparison for the $D^{(*)}$ mesons as well. For the quark masses in Eq. (47) the values of $\overline{m}_b(m_b) = 4.2\,\mathrm{GeV}$ and $\overline{m}_c(m_b) = 1.1\,\mathrm{GeV}$ were used. The plot shows for each hadronic final state $R(X)/R(X)\big|_{\rm SM}$ as a function of $\tan\beta/m_{H^\pm}$. While to such scalar currents the sensitivity of the $B\to D\ell\bar\nu$ appears to be the best, that is not generic for all new physics scenarios. The lower plot in Fig. 4 shows the ratios of τ to light-lepton rates as functions of $S_R - S_L$ for $S_R + S_L = 0.25$ for the D^*, D_0^*, and D_2^* final states. The rates to the other three states we consider only depend on $S_R + S_L$ [see Eq. (47)], so those are not plotted. This scenario is motivated by being able to fit, besides $R(D^{(*)})$, the q^2 spectrum measured in Ref. [2] as well. The vertical blue shaded bands show the best fit regions [2]. Measurements of $R(D^{**})$ can help discriminate between the currently allowed solutions of S_L and S_R, and also distinguish more complex scenarios.

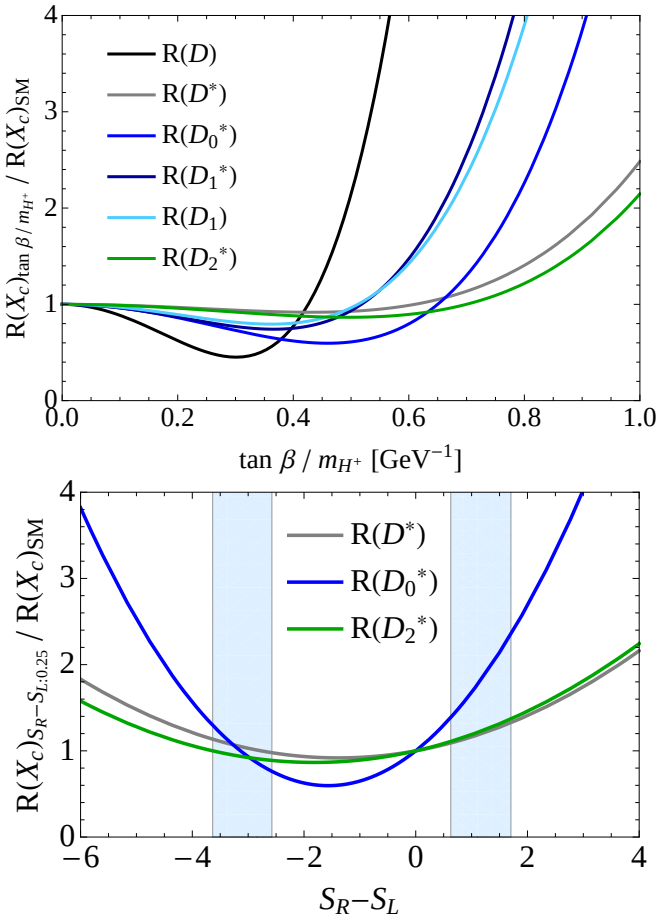

FIG. 4. Upper plot: Ratios of τ to light-lepton rates in the type-II 2HDM, as functions of $\tan\beta/m_{H^\pm}$. For the four D^{**} states and the two $D^{(*)}$ mesons $R(X)/R(X)\big|_{\rm SM}$ is shown as functions of $\tan\beta/m_{H^\pm}$. Lower plot: Ratios of τ to light-lepton rates as functions of $S_R - S_L$, for $S_R + S_L = 0.25$, for D^*, D_0^*, and D_2^* final states. The vertical blue shaded bands show the allowed regions for $S_R - S_L$ as measured in Ref. [2].

VI. SUMMARY AND CONCLUSIONS

We performed the first model independent study of semileptonic $B\to D^{**}\ell\bar\nu$ decays based on heavy quark symmetry, including the full dependence on the charged lepton mass. This is important, because future measurements of $R(D^{**})$ give complementary sensitivity to new physics than $R(D^{(*)})$. It is also important to better understand the semileptonic $B\to D^{**}$ decays in the zero lepton mass channels, which are significant contributions to the systematic uncertainties for the measurements of $|V_{cb}|$ and $|V_{ub}|$, in addition to $R(D^{(*)})$.

There are at least two measurements which could be done with existing data, that would add substantially to our understanding of D^{**} states and the decays discussed in this paper: (1) The nonleptonic $B\to D^{**}\pi$ rates have only been measured with small fractions of the *BABAR* and Belle data, and are the sources of tensions. Redoing these measurements with the full data sets would be important. (2) In the strange sector, one should revisit the ratio $\mathcal{B}(D_{s0}\to D_s^*\gamma)/\mathcal{B}(D_{s0}\to D_s\pi)$, for which CLEO obtained a ~ 3 times stronger upper bound than *BABAR* and Belle, and the latter experiments have much more

data not yet analyzed for this ratio.

Our main results for $R(D^{**})$ are Eqs. (34) and the even more conservative Eqs. (38). The precision of these predictions can be improved in a straightforward manner in the future, with more precise measurements of the differential decay rates in the e and μ modes. That will allow to better constrain the (relevant combinations of) subleading Isgur-Wise functions, thereby reducing the uncertainty of $R(D^{**})$. Measuring the e and μ modes should be high priority also for their potential impacts on reducing the uncertainties in $|V_{cb}|$ and $|V_{ub}|$ measurements.

For the semi-tauonic rate to the sum of four states we obtain $\mathcal{B}(B \to D^{**}\tau\bar{\nu}) = (0.14 \pm 0.03)\%$. This is smaller than the estimate in Ref. [6]; nevertheless, it sharpens the tension between the data on the inclusive and sum over exclusive $b \to c\tau\bar{\nu}$ mediated rates.

ACKNOWLEDGMENTS

We thank Michele Papucci, Dean Robinson, Marcello Rotondo and Sheldon Stone for helpful conversations. FB thanks Niklas and Nicole Wicki for good conversations in Zermatt, where parts of this manuscript were worked out. Special thanks to Stephan Duell to point out a typo in the helicity amplitude formulae in the appendix. ZL thanks the hospitality of the Aspen Center for Physics, supported by the NSF Grant No. PHY-1066293. ZL was supported in part by the Office of Science, Office of High Energy Physics, of the U.S. Department of Energy under contract DE-AC02-05CH11231.

Appendix A: LLSW Form Factor expansion

The used mass splittings and quark masses are listed in Table IV. The ratios, $\varepsilon_{c,b} = 1/(2m_{c,b})$, and the subleading Isgur-Wise functions $\tau_{1/2/3}$ also enter the form factor expansion. Here $\tau_{1/2}$ and $\tau_{3/2}$ are the leading Isgur-Wise function of the $s_l^\pi = \frac{1}{2}^+$ and $s_l^\pi = \frac{3}{2}^+$ states, respectively. Below, we repeat for completeness the expansion of the form factors to order $1/m_{c,b}$ [8, 9].

The form factors for $B \to D_0^* \ell\,\bar{\nu}$ are

$$\begin{aligned} g_+ &= \varepsilon_c\Big[2(w-1)\zeta_1 - 3\zeta\,\frac{w\bar{\Lambda}^* - \bar{\Lambda}}{w+1}\Big] \\ &\quad - \varepsilon_b\Big[\frac{\bar{\Lambda}^*(2w+1) - \bar{\Lambda}(w+2)}{w+1}\,\zeta - 2(w-1)\,\zeta_1\Big], \\ g_- &= \zeta + \varepsilon_c\Big[\chi_{\rm ke} + 6\chi_1 - 2(w+1)\chi_2\Big] + \varepsilon_b\,\chi_b\,. \end{aligned} \tag{A1}$$

The form factors for $B \to D_1^* \ell\,\bar{\nu}$ are

$$\begin{aligned} g_A &= \zeta + \varepsilon_c\Big[\frac{w\bar{\Lambda}^* - \bar{\Lambda}}{w+1}\zeta + \chi_{\rm ke} - 2\chi_1\Big] - \varepsilon_b\,\Big[\frac{\bar{\Lambda}^*(2w+1) - \bar{\Lambda}(w+2)}{w+1}\,\zeta - 2(w-1)\,\zeta_1 - \chi_b\Big], \\ g_{V_1} &= (w-1)\zeta + \varepsilon_c\Big[(w\bar{\Lambda}^* - \bar{\Lambda})\zeta + (w-1)(\chi_{\rm ke} - 2\chi_1)\Big] - \varepsilon_b\Big\{\big[\bar{\Lambda}^*(2w+1) - \bar{\Lambda}(w+2)\big]\zeta - 2(w^2-1)\zeta_1 - (w-1)\chi_b\Big\}, \\ g_{V_2} &= 2\varepsilon_c\,(\zeta_1 - \chi_2)\,, \\ g_{V_3} &= -\zeta - \varepsilon_c\Big[\frac{w\bar{\Lambda}^* - \bar{\Lambda}}{w+1}\zeta + 2\zeta_1 + \chi_{\rm ke} - 2\chi_1 + 2\chi_2\Big] + \varepsilon_b\Big[\frac{\bar{\Lambda}^*(2w+1) - \bar{\Lambda}(w+2)}{w+1}\,\zeta - 2(w-1)\,\zeta_1 - \chi_b\Big]. \end{aligned} \tag{A2}$$

The form factors for $B \to D_1 \ell\,\bar{\nu}$ are

$$\begin{aligned} \sqrt{6}\,f_A &= -(w+1)\tau - \varepsilon_b\big\{(w-1)\big[(\bar{\Lambda}' + \bar{\Lambda})\tau - (2w+1)\tau_1 - \tau_2\big] + (w+1)\eta_b\big\} \\ &\quad - \varepsilon_c\big[4(w\bar{\Lambda}' - \bar{\Lambda})\tau - 3(w-1)(\tau_1 - \tau_2) + (w+1)(\eta_{\rm ke} - 2\eta_1 - 3\eta_3)\big]\,, \\ \sqrt{6}\,f_{V_1} &= (1-w^2)\tau - \varepsilon_b(w^2-1)\big[(\bar{\Lambda}' + \bar{\Lambda})\tau - (2w+1)\tau_1 - \tau_2 + \eta_b\big] \\ &\quad - \varepsilon_c\big[4(w+1)(w\bar{\Lambda}' - \bar{\Lambda})\tau - (w^2-1)(3\tau_1 - 3\tau_2 - \eta_{\rm ke} + 2\eta_1 + 3\eta_3)\big]\,, \\ \sqrt{6}\,f_{V_2} &= -3\tau - 3\varepsilon_b\big[(\bar{\Lambda}' + \bar{\Lambda})\tau - (2w+1)\tau_1 - \tau_2 + \eta_b\big] \\ &\quad - \varepsilon_c\big[(4w-1)\tau_1 + 5\tau_2 + 3\eta_{\rm ke} + 10\eta_1 + 4(w-1)\eta_2 - 5\eta_3\big]\,, \\ \sqrt{6}\,f_{V_3} &= (w-2)\tau + \varepsilon_b\big\{(2+w)\big[(\bar{\Lambda}' + \bar{\Lambda})\tau - (2w+1)\tau_1 - \tau_2\big] - (2-w)\eta_b\big\} \\ &\quad + \varepsilon_c\big[4(w\bar{\Lambda}' - \bar{\Lambda})\tau + (2+w)\tau_1 + (2+3w)\tau_2 \\ &\quad\quad + (w-2)\eta_{\rm ke} - 2(6+w)\eta_1 - 4(w-1)\eta_2 - (3w-2)\eta_3\big]\,. \end{aligned} \tag{A3}$$

The form factors for $B \to D_2^* \ell\,\bar{\nu}$ are

$$\begin{aligned} k_V &= -\tau - \varepsilon_b\big[(\bar{\Lambda}' + \bar{\Lambda})\tau - (2w+1)\tau_1 - \tau_2 + \eta_b\big] - \varepsilon_c(\tau_1 - \tau_2 + \eta_{\rm ke} - 2\eta_1 + \eta_3)\,, \\ k_{A_1} &= -(1+w)\tau - \varepsilon_b\big\{(w-1)\big[(\bar{\Lambda}' + \bar{\Lambda})\tau - (2w+1)\tau_1 - \tau_2\big] + (1+w)\eta_b\big\} \\ &\quad - \varepsilon_c\big[(w-1)(\tau_1 - \tau_2) + (w+1)(\eta_{\rm ke} - 2\eta_1 + \eta_3)\big]\,, \end{aligned}$$

$$k_{A_2} = -2\varepsilon_c(\tau_1 + \eta_2)\,,$$
$$k_{A_3} = \tau + \varepsilon_b\big[(\bar\Lambda' + \bar\Lambda)\tau - (2w+1)\tau_1 - \tau_2 + \eta_b\big] - \varepsilon_c(\tau_1 + \tau_2 - \eta_{\rm ke} + 2\eta_1 - 2\eta_2 - \eta_3)\,. \tag{A4}$$

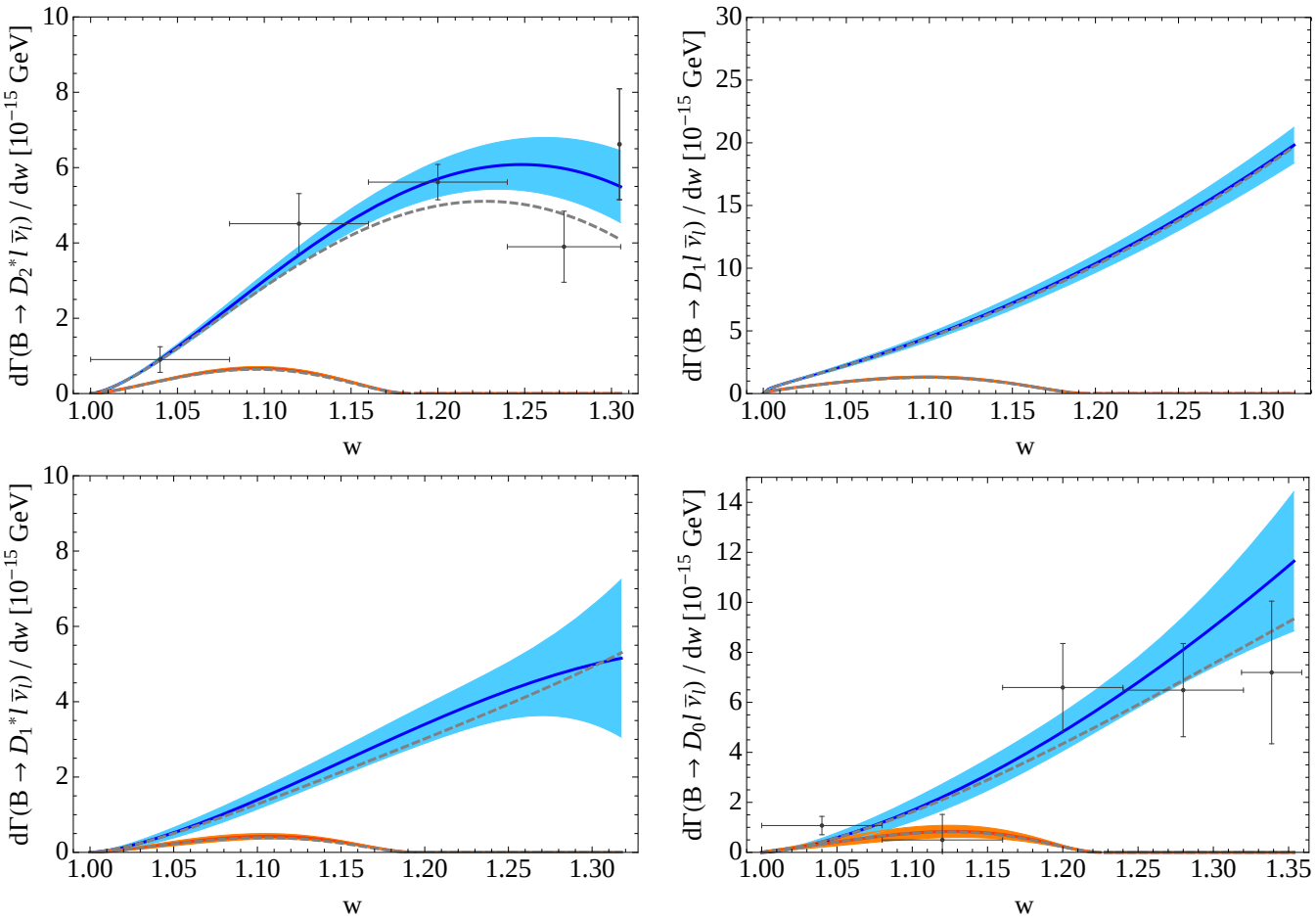

FIG. 5. The colored bands show the allowed 68% regions for $m_\ell = 0$ (blue) and $m_\ell = m_\tau$ (orange) for the differential decay rates in Approximation A. The dashed curves show the predictions of Ref. [9]. The data points correspond to the differential semileptonic or nonleptonic branching fraction measurements described in the text.

Appendix B: Approximation A

We attempt to keep the definition as similar to Ref. [9] as possible. In light of Eqs. (9)–(11), we factor out $(1-2rw+r^2-\rho_\ell)^2/(1-2rw+r^2)^2$, which reduces to 1 in the $\rho_\ell \to 0$ limit. Expanding in powers of $w-1$, we write for the $\frac{3}{2}^+$ states,

$$\frac{{\rm d}\Gamma_{D_1}}{{\rm d}w\,{\rm d}\cos\theta} = \Gamma_0\,\tau^2(1)\,r^3\,\sqrt{w^2-1}\,\frac{(1-2rw+r^2-\rho_\ell)^2}{(1-2rw+r^2)^2}\sum_n (w-1)^n\Big\{\sin^2\theta\,s_1^{(n)} + (1-2rw+r^2)\Big[(1+\cos^2\theta)\,t_1^{(n)} - 4\cos\theta\,\sqrt{w^2-1}\,u_1^{(n)}\Big]\Big\}\,, \tag{B1}$$

$$\frac{{\rm d}\Gamma_{D_2^*}}{{\rm d}w\,{\rm d}\cos\theta} = \frac{3}{2}\,\Gamma_0\,\tau^2(1)\,r^3\,(w^2-1)^{3/2}\,\frac{(1-2rw+r^2-\rho_\ell)^2}{(1-2rw+r^2)^2}\sum_n (w-1)^n\Big\{\frac{4}{3}\sin^2\theta\,s_2^{(n)} + (1-2rw+r^2)\Big[(1+\cos^2\theta)\,t_2^{(n)} - 4\cos\theta\,\sqrt{w^2-1}\,u_2^{(n)}\Big]\Big\}\,, \tag{B2}$$

and for the $\frac{1}{2}^+$ states,

$$\frac{\mathrm{d}\Gamma_{D_0^*}}{\mathrm{d}w\,\mathrm{d}\cos\theta} = 3\Gamma_0\,\zeta^2(1)\,r^3\,\sqrt{w^2-1}\,\frac{(1-2rw+r^2-\rho_\ell)^2}{(1-2rw+r^2)^2}\,\sum_n (w-1)^n\left\{\sin^2\theta\, s_0^{(n)} + \left[(1+\cos^2\theta)\,t_0^{(n)} - 4\cos\theta\,\sqrt{w^2-1}\,u_0^{(n)}\right]\right\}, \tag{B3}$$

$$\frac{\mathrm{d}\Gamma_{D_1^*}}{\mathrm{d}w\,\mathrm{d}\cos\theta} = 3\Gamma_0\,\zeta^2(1)\,r^3\,\sqrt{w^2-1}\,\frac{(1-2rw+r^2-\rho_\ell)^2}{(1-2rw+r^2)^2}\,\sum_n (w-1)^n\left\{\sin^2\theta\, s_{1*}^{(n)} + (1-2rw+r^2)\left[(1+\cos^2\theta)\,t_{1*}^{(n)} - 4\cos\theta\,\sqrt{w^2-1}\,u_{1*}^{(n)}\right]\right\}. \tag{B4}$$

The structure of the expansion for D_0^* changes for $\rho_\ell \neq 0$ compared to Ref. [9], where $(w^2-1)^{3/2}$ occurred before the sum in the analog of Eq. (B3). One power of (w^2-1) suppression is eliminated for $\rho_\ell \neq 0$. In Eq. (B3), $s_0^{(0)}$, $t_0^{(n)}$, and $u_0^{(n)}$ are proportional to ρ_ℓ, and $s_0^{(1,2)}$ correspond to $s_0^{(0,1)}$ in Ref. [9]. For the decays to D_1^*, D_1, and D_2^*, Approximation A in this paper coincides with Ref. [9] in the $\rho_\ell \to 0$ limit, while for D_0^* there is this small difference, which is higher order in $w-1$.[3]

The subscripts of the coefficients s, t, u denote the spin of the excited D meson, while the superscripts refer to the order in the $w-1$ expansion. The $u_i^{(n)}$ terms proportional to $\cos\theta$ only affect the lepton spectrum, since they vanish when integrated over θ. (We do not expand the factors of $\sqrt{w^2-1}$ multiplying these $\cos\theta$ terms.)

We obtain for the coefficients in the D_1 decay rate

$$\begin{aligned}
s_1^{(0)} &= 16\varepsilon_c^2\,(\bar\Lambda'-\bar\Lambda)^2\left[2(1-r)^2+\rho_\ell\right] + \mathcal{O}(\rho_\ell^2\varepsilon^2,\,\varepsilon^3)\,,\\
s_1^{(1)} &= 12\rho_\ell + 32\varepsilon_c(\bar\Lambda'-\bar\Lambda)\big(1-r^2+\rho_\ell\big)\\
&\quad + 8\rho_\ell\big[\varepsilon_c(3\hat\eta_{\rm ke}+10\hat\eta_1-5\hat\eta_3)+3\varepsilon_b\hat\eta_b\big] + \mathcal{O}(\rho_\ell^2\varepsilon,\,\varepsilon^2),\\
s_1^{(2)} &= 8\,(1+r)^2 + 8\rho_\ell\,(2+3\hat\tau') + \mathcal{O}(\rho_\ell^2,\,\varepsilon)\,,\\
t_1^{(0)} &= 16\varepsilon_c^2\,(\bar\Lambda'-\bar\Lambda)^2\left[2+\frac{\rho_\ell}{(1-r)^2}\right] + \mathcal{O}(\rho_\ell^2\varepsilon^2,\,\varepsilon^3)\,,\\
t_1^{(1)} &= 4\left[1+\frac{2\rho_\ell}{(1-r)^2}\right]\big[1+2\varepsilon_c(\hat\eta_{\rm ke}-2\hat\eta_1-3\hat\eta_3)+2\varepsilon_b\hat\eta_b\big]\\
&\quad + 32\varepsilon_c(\bar\Lambda'-\bar\Lambda)\left[1+\frac{\rho_\ell(1+r)}{(1-r)^3}\right] + 32\varepsilon_c\rho_\ell\frac{4\hat\eta_1+\hat\eta_3}{(1-r)^2}\\
&\quad + \mathcal{O}(\rho_\ell^2\varepsilon,\,\varepsilon^2)\,,\\
t_1^{(2)} &= 8\,(1+\hat\tau') + 16\rho_\ell\left[\frac{1+\hat\tau'}{(1-r)^2}+\frac{3r}{(1-r)^4}\right] + \mathcal{O}(\rho_\ell^2,\,\varepsilon)\,,\\
u_1^{(0)} &= 8\varepsilon_c\,(\bar\Lambda'-\bar\Lambda)\left[1-\frac{\rho_\ell}{(1-r)^2}\right]^2 + \mathcal{O}(\varepsilon^2)\,,\\
u_1^{(1)} &= 2-4\rho_\ell\,\frac{1+r}{(1-r)^3} + \mathcal{O}(\rho_\ell^2,\,\varepsilon)\,,
\end{aligned} \tag{B5}$$

where ε^n denotes any term of the form $\varepsilon_c^m\varepsilon_b^{n-m}$, with $n,\, n-m \geq 0$. For the decay rate into D_2^*, the first two terms in the $w-1$ expansion are

$$\begin{aligned}
s_2^{(0)} &= \big[4(1-r)^2+\rho_\ell\big]\big[1+2\varepsilon_c\,(\hat\eta_{\rm ke}-2\hat\eta_1+\hat\eta_3)+2\varepsilon_b\,\hat\eta_b\big]\\
&\quad + \mathcal{O}(\rho_\ell^2\varepsilon,\,\varepsilon^2)\,,\\
s_2^{(1)} &= 4\,(1-r)^2(1+2\hat\tau') + \rho_\ell\left(\frac{7}{2}+2\hat\tau'\right) + \mathcal{O}(\rho_\ell^2,\,\varepsilon)\,,\\
t_2^{(0)} &= 4\big[1+2\varepsilon_b\,\hat\eta_b+2\varepsilon_c(\hat\eta_{\rm ke}-2\hat\eta_1+\hat\eta_3)\big]\left[1+\frac{2\rho_\ell}{3(1-r)^2}\right]\\
&\quad + \mathcal{O}(\rho_\ell^2,\,\varepsilon)\,,\\
t_2^{(1)} &= 2(3+4\hat\tau') + 4\rho_\ell\left[\frac{(1+r)^2}{(1-r)^4}+\frac{4\hat\tau'}{3(1-r)^2}\right] + \mathcal{O}(\rho_\ell^2,\,\varepsilon)\,,\\
u_2^{(0)} &= 2-\rho_\ell\,\frac{4(1+r)}{3(1-r)^3} + \mathcal{O}(\rho_\ell^2,\,\varepsilon)\,.
\end{aligned} \tag{B6}$$

Note that aiming at higher accuracy for the D_2^* rate by keeping the $s_2^{(2)}$ and $t_2^{(2)}$ coefficients, even at leading order, would introduce a new parameter, $\tau''(1)$, hence reducing the simplicity of this approximation (besides deviating from the "power counting").

For the decay rate into D_0^* we get

$$\begin{aligned}
s_0^{(0)} &= \frac{9\,\rho_\ell}{2}\,(\varepsilon_c+\varepsilon_b)^2\,(\bar\Lambda^*-\bar\Lambda)^2 + \mathcal{O}(\rho_\ell^2\varepsilon^2,\,\rho_\ell\varepsilon^3)\,,\\
s_0^{(1)} &= \big[2(1-r)^2-\rho_\ell\big]\big[1+2\varepsilon_c(\hat\chi_{\rm ke}+6\hat\chi_1-4\hat\chi_2)+2\varepsilon_b\hat\chi_b\big]\\
&\quad + 6(\varepsilon_c+\varepsilon_b)(\bar\Lambda^*-\bar\Lambda)\,(1-r^2) + \mathcal{O}(\rho_\ell^2\varepsilon,\,\varepsilon^2)\,,\\
s_0^{(2)} &= (1-r)^2\,(1+4\hat\zeta') - 2\,\rho_\ell\,\hat\zeta' + \mathcal{O}(\rho_\ell^2,\,\varepsilon)\,.\\
t_0^{(0)} &= \frac{9\,\rho_\ell}{2}\,(\varepsilon_c+\varepsilon_b)^2\,(\bar\Lambda^*-\bar\Lambda)^2 + \mathcal{O}(\rho_\ell^2\varepsilon^2,\,\rho_\ell\varepsilon^3)\,,\\
t_0^{(1)} &= \rho_\ell\,\big[1+2\varepsilon_c(\hat\chi_{\rm ke}+6\hat\chi_1-4\hat\chi_2)+2\varepsilon_b\hat\chi_b\big]\\
&\quad + 6\rho_\ell\,(\varepsilon_c+\varepsilon_b)\,(\bar\Lambda^*-\bar\Lambda)\,\frac{1+r}{1-r} + \mathcal{O}(\rho_\ell^2\varepsilon,\,\rho_\ell\varepsilon^2),\\
t_0^{(2)} &= \rho_\ell\left[2\hat\zeta'+\frac{(1+r)^2}{(1-r)^2}\right] + \mathcal{O}(\rho_\ell^2,\,\rho_\ell\varepsilon)\,,\\
u_0^{(0)} &= -\frac{3\,\rho_\ell}{2(1-r)^2}\,(\varepsilon_c+\varepsilon_b)\,(\bar\Lambda^*-\bar\Lambda) + \mathcal{O}(\rho_\ell^2\varepsilon,\,\rho_\ell\varepsilon^2)\,,
\end{aligned}$$

[3] In Ref. [9] there is a typo in the $s_0^{(0)}$ coefficient in Eq. (3.18): the $4\varepsilon_b\hat\chi_b$ term should read $2\varepsilon_b\hat\chi_b$, since $\varepsilon_c\hat\chi_{\rm ke}$ and $\varepsilon_b\hat\chi_b$ must have the same coefficients. This is corrected in $s_0^{(1)}$ in Eq. (B7) below; note the shift of the upper index by 1, as explained above.

$$u_0^{(1)} = -\frac{\rho_\ell\,(1+r)}{2(1-r)^3} + \mathcal{O}(\rho_\ell^2,\, \rho_\ell\varepsilon)\,. \tag{B7}$$

For the decay into D_1^* the coefficients are

$$\begin{aligned}
s_{1*}^{(0)} &= (\varepsilon_c - 3\varepsilon_b)^2\,(\bar\Lambda^* - \bar\Lambda)^2\left[(1-r)^2 + \frac{\rho_\ell}{2}\right] + \mathcal{O}(\rho_\ell^2\varepsilon^2,\, \varepsilon^3),\\
s_{1*}^{(1)} &= 3\rho_\ell - 2(\varepsilon_c - 3\varepsilon_b)\,(\bar\Lambda^* - \bar\Lambda)\big[(1-r^2) - 2\rho_\ell\big]\\
&\quad + 2\rho_\ell\big[\varepsilon_c(3\hat\chi_{\rm ke} - 6\hat\chi_1 + 4\hat\chi_2) + 3\varepsilon_b\hat\chi_b\big] + \mathcal{O}(\rho_\ell^2\varepsilon,\, \varepsilon^2),\\
s_{1*}^{(2)} &= (1+r)^2 + \rho_\ell\,(2 + 6\hat\zeta') + \mathcal{O}(\rho_\ell^2,\, \varepsilon)\,,\\
t_{1*}^{(0)} &= (\varepsilon_c - 3\varepsilon_b)^2\,(\bar\Lambda^* - \bar\Lambda)^2\left[1 + \frac{\rho_\ell}{2(1-r)^2}\right] + \mathcal{O}(\rho_\ell^2\varepsilon,\, \varepsilon^2)\,,\\
t_{1*}^{(1)} &= \left[2 + \frac{\rho_\ell}{(1-r)^2}\right]\big[1 + 2\varepsilon_c(\hat\chi_{\rm ke} - 2\hat\chi_1) + 2\varepsilon_b\hat\chi_b\big]\\
&\quad + 2(\varepsilon_c - 3\varepsilon_b)(\bar\Lambda^* - \bar\Lambda)\left[2 - \frac{\rho_\ell(1+r)}{(1-r)^3}\right]\\
&\quad + \varepsilon_c\frac{8\rho_\ell\,\hat\chi_2}{(1-r)^2} + \mathcal{O}(\rho_\ell^2\varepsilon,\, \varepsilon^2)\,,\\
t_{1*}^{(2)} &= 2 + 4\hat\zeta' + \rho_\ell\left[\frac{1+4r+r^2}{(1-r)^4} + \frac{2\hat\zeta'}{(1-r)^2}\right] + \mathcal{O}(\rho_\ell^2,\, \varepsilon)\,,\\
u_{1*}^{(0)} &= (\varepsilon_c - 3\varepsilon_b)(\bar\Lambda^* - \bar\Lambda)\left[1 + \frac{\rho_\ell}{2(1-r)^2}\right] + \mathcal{O}(\rho_\ell^2\varepsilon,\, \varepsilon^2)\,,\\
u_{1*}^{(1)} &= 1 - \frac{\rho_\ell\,(1+r)}{2(1-r)^3} + \mathcal{O}(\rho_\ell^2,\, \varepsilon)\,.
\end{aligned} \tag{B8}$$

Figure 5 compares the differential decay rates in Approximation A using the fitted values for the narrow and broad Isgur-Wise function parametrization in Table VIII with Ref. [9].

Appendix C: Helicity amplitudes

1. Helicity amplitudes for $B \to D_0^*\,\ell\bar\nu$

The $H_\pm$ helicity amplitudes vanish for semileptonic decays to scalar final state mesons, and only the zero helicity amplitudes, H_0 and H_t contribute to the decay rate,

$$H_\pm^S = 0\,, \tag{C1}$$

$$H_0^S = -\frac{m_B\sqrt{r}}{\sqrt{q^2}}\,|\vec p\,'|\left[\left(1+\frac{1}{r}\right)f_+ + \left(1-\frac{1}{r}\right)f_-\right], \tag{C2}$$

$$H_t^S = -\frac{m_B\sqrt{r}}{\sqrt{q^2}}\,\big(t_+\,f_+ + t_-\,f_-\big), \tag{C3}$$

with $r = m_{D^{**}}/m_B$, $t_\pm = m_B \mp m_{D^{**}} - E'(1 \mp 1/r) = m_B - E' \mp (m_B\,r - E'/r)$, and E' denotes the energy of the D^{**} meson in the B rest frame.

2. Helicity amplitudes for $B \to D_1\,\ell\bar\nu$ and $D_1^*\,\ell\bar\nu$

For vector final state mesons all four helicity amplitudes contribute:

$$H_\pm^V = m_B\sqrt{r}\,f_{V_1} \mp \frac{1}{\sqrt{r}}\,|\vec p\,'|\,f_A\,, \tag{C4}$$

$$H_0^V = \frac{1}{\sqrt{r\,q^2}}\left[m_B(E' - m_B r^2)\,f_{V_1} + \frac{|\vec p\,'|^2}{r}\big(r f_{V_2} + f_{V_3}\big)\right], \tag{C5}$$

$$H_t^V = m_B\,\frac{|\vec p\,'|}{\sqrt{r\,q^2}}\left[f_{V_1} + \left(1 - \frac{E'}{m_B}\right)f_{V_2} + \left(\frac{E'}{m_B\,r} - r\right)f_{V_3}\right]. \tag{C6}$$

The helicity amplitudes for D_1^* can be obtained by the replacements $f_{V_1,V_2,V_3,A} \to g_{V_1,V_2,V_3,A}$.

3. Helicity amplitudes for $B \to D_2^*\,\ell\bar\nu$

For tensor final states also all four helicity amplitudes contribute:

$$H_\pm^T = \mp\frac{1}{\sqrt{2\,r}}\,\frac{|\vec p\,'|^2}{m_B r}\,k_V - \frac{1}{\sqrt{2\,r}}\,|\vec p\,'|\,k_{A_1}\,, \tag{C7}$$

$$\begin{aligned}
H_0^T &= \sqrt{\frac{2}{3}}\,\frac{|\vec p\,'|}{\sqrt{r^3\,q^2}}\left[(E' - m_B\,r^2)\,k_{A_1}\right.\\
&\quad \left. + \frac{|\vec p\,'|^2}{m_B}\left(k_{A_2} + \frac{1}{r}\,k_{A_3}\right)\right],
\end{aligned} \tag{C8}$$

$$H_t^T = \sqrt{\frac{2}{3}}\,\frac{|\vec p\,'|^2}{\sqrt{r^3\,q^2}}\left[k_{A_1} + \left(1 - \frac{E'}{m_B}\right)k_{A_2} + \left(\frac{E'}{m_B\,r} - r\right)k_{A_3}\right]. \tag{C9}$$

[1] J. P. Lees *et al.* [BaBar Collaboration], Phys. Rev. Lett. **109**, 101802 (2012) [arXiv:1205.5442 [hep-ex]].

[2] J. P. Lees *et al.* [BaBar Collaboration], Phys. Rev. D **88**, no. 7, 072012 (2013) [arXiv:1303.0571 [hep-ex]].

[3] M. Huschle *et al.* [Belle Collaboration], [arXiv:1507.03233 [hep-ex]].

[4] R. Aaij *et al.* [LHCb Collaboration], Phys. Rev. Lett. **115**, no. 11, 111803 (2015) [arXiv:1506.08614 [hep-ex]].

[5] Heavy Flavor Averaging Group, Y. Amhis *et al.*, arXiv:1412.7515; and updates at `http://www.slac.stanford.edu/xorg/hfag/`.

[6] M. Freytsis, Z. Ligeti and J. T. Ruderman, Phys. Rev. D **92**, no. 5, 054018 (2015) [arXiv:1506.08896 [hep-ph]].

[7] N. Isgur and M. B. Wise, "Weak Decays of Heavy Mesons in the Static Quark Approximation," Phys. Lett. B **232**, 113 (1989); "Weak Transition Form-factors Between Heavy Mesons," Phys. Lett. B **237**, 527 (1990).

[8] A. K. Leibovich, Z. Ligeti, I. W. Stewart and M. B. Wise, Phys. Rev. Lett. **78**, 3995 (1997) [hep-ph/9703213].

[9] A. K. Leibovich, Z. Ligeti, I. W. Stewart and M. B. Wise, Phys. Rev. D **57**, 308 (1998) [hep-ph/9705467].

[10] R. Aaij *et al.* [LHCb Collaboration], JHEP **1309**, 145 (2013) [arXiv:1307.4556].

[11] R. Aaij *et al.* [LHCb Collaboration], JHEP **1504**, 024 (2015) [arXiv:1502.02638 [hep-ex]].

[12] N. Isgur and M. B. Wise, Phys. Rev. Lett. **66**, 1130 (1991).

[13] J. M. Link *et al.* [FOCUS Collaboration], Phys. Lett. B **586**, 11 (2004) [hep-ex/0312060].

[14] K. Abe *et al.* [Belle Collaboration], Phys. Rev. D **69**, 112002 (2004) [hep-ex/0307021].

[15] B. Aubert *et al.* [BaBar Collaboration], Phys. Rev. D **79**, 112004 (2009) [arXiv:0901.1291 [hep-ex]].

[16] R. Aaij *et al.* [LHCb Collaboration], Phys. Rev. D **92**, no. 1, 012012 (2015) [arXiv:1505.01505 [hep-ex]].

[17] R. Klein, T. Mannel, F. Shahriaran and D. van Dyk, Phys. Rev. D **91**, no. 9, 094034 (2015) [arXiv:1503.00569 [hep-ph]].

[18] M. Lu, M. B. Wise and N. Isgur, Phys. Rev. D **45**, 1553 (1992).

[19] U. Kilian, J. G. Korner and D. Pirjol, Phys. Lett. B **288**, 360 (1992).

[20] A. F. Falk and T. Mehen, Phys. Rev. D **53**, 231 (1996) [hep-ph/9507311].

[21] P. Biancofiore, P. Colangelo and F. De Fazio, Phys. Rev. D **87**, no. 7, 074010 (2013) [arXiv:1302.1042 [hep-ph]].

[22] N. Isgur, D. Scora, B. Grinstein and M. B. Wise, Phys. Rev. D **39**, 799 (1989); D. Scora and N. Isgur, Phys. Rev. D **52**, 2783 (1995) [hep-ph/9503486].

[23] P. Colangelo, G. Nardulli and N. Paver, Phys. Lett. B **293**, 207 (1992).

[24] S. Veseli and M. G. Olsson, Phys. Rev. D **54**, 886 (1996) [hep-ph/9601307]; Phys. Lett. B **367**, 302 (1996) [hep-ph/9507425].

[25] V. Morenas, A. Le Yaouanc, L. Oliver, O. Pene and J. C. Raynal, Phys. Rev. D **56**, 5668 (1997) [hep-ph/9706265]; Phys. Lett. B **386**, 315 (1996) [hep-ph/9605206].

[26] N. Isgur and M. B. Wise, Phys. Rev. D **43**, 819 (1991).

[27] B. Blossier *et al.* [European Twisted Mass Collaboration], JHEP **0906**, 022 (2009) [arXiv:0903.2298 [hep-lat]].

[28] M. Atoui, B. Blossier, V. Mornas, O. Pne and K. Petrov, Eur. Phys. J. C **75**, no. 8, 376 (2015) [arXiv:1312.2914 [hep-lat]].

[29] F. U. Bernlochner, Phys. Rev. D **92**, no. 11, 115019 (2015) [arXiv:1509.06938 [hep-ph]].

[30] D. Liventsev *et al.* [Belle Collaboration], Phys. Rev. D **77**, 091503 (2008) [arXiv:0711.3252 [hep-ex]].

[31] B. Aubert *et al.* [BaBar Collaboration], Phys. Rev. Lett. **101**, 261802 (2008) [arXiv:0808.0528 [hep-ex]].

[32] K. A. Olive *et al.* [Particle Data Group], Chin. Phys. C **38**, 090001 (2014).

[33] R. Aaij *et al.* [LHCb Collaboration], Phys. Rev. D **84**, 092001 (2011) [Phys. Rev. D **85**, 039904 (2012)] [arXiv:1109.6831 [hep-ex]].

[34] J. P. Lees *et al.* [BaBar Collaboration], Phys. Rev. Lett. **116**, no. 4, 041801 (2016) [arXiv:1507.08303 [hep-ex]].

[35] K. Abe *et al.* [Belle Collaboration], Phys. Rev. Lett. **94**, 221805 (2005) [hep-ex/0410091].

[36] M. Neubert, Phys. Lett. B **418**, 173 (1998) [hep-ph/9709327].

[37] C. W. Bauer, D. Pirjol and I. W. Stewart, Phys. Rev. Lett. **87**, 201806 (2001) [hep-ph/0107002].

[38] F. Jugeau, A. Le Yaouanc, L. Oliver and J.-C. Raynal, Phys. Rev. D **72**, 094010 (2005) [hep-ph/0504206].

[39] I. I. Bigi, B. Blossier, A. Le Yaouanc, L. Oliver, O. Pene, J.-C. Raynal, A. Oyanguren and P. Roudeau, Eur. Phys. J. C **52**, 975 (2007) [arXiv:0708.1621 [hep-ph]]; and references therein.

[40] S. Mantry, Phys. Rev. D **70**, 114006 (2004) [hep-ph/0405290].

[41] B. Aubert *et al.* [BaBar Collaboration], Phys. Rev. Lett. **90**, 242001 (2003) [hep-ex/0304021].

[42] L. Leskovec, C. B. Lang, D. Mohler, S. Prelovsek and R. M. Woloshyn, arXiv:1511.04140 [hep-lat].

[43] S. Godfrey, Phys. Lett. B **568**, 254 (2003) [hep-ph/0305122].

[44] P. Colangelo and F. De Fazio, Phys. Lett. B **570**, 180 (2003) [hep-ph/0305140].

[45] T. Mehen and R. P. Springer, Phys. Rev. D **70**, 074014 (2004) [hep-ph/0407181].

[46] D. Besson *et al.* [CLEO Collaboration], Phys. Rev. D **68**, 032002 (2003) Erratum: [Phys. Rev. D **75**, 119908 (2007)] [hep-ex/0305100].

[47] S.-K. Choi *et al.* [Belle Collaboration], Phys. Rev. D **91**, no. 9, 092011 (2015) Addendum: [Phys. Rev. D **92**, no. 3, 039905 (2015)] [arXiv:1504.02637 [hep-ex]].

[48] K. Abe *et al.* [Belle Collaboration], Phys. Rev. Lett. **92**, 012002 (2004) [hep-ex/0307052].

[49] B. Aubert *et al.* [BaBar Collaboration], Phys. Rev. D **74**, 032007 (2006) [hep-ex/0604030].

[50] R. Aaij *et al.* [LHCb Collaboration], JHEP **1602**, 133 (2016) [arXiv:1601.01495 [hep-ex]].

[51] J. G. Korner and G. A. Schuler, Z. Phys. C **46**, 93 (1990).